Enhancement of the Spatial Resolution for the Temperature Sensing System of the 7 Tesla Magnetic Resonance Imaging Scanner

Tariq Saboerali

Master of Science Thesis

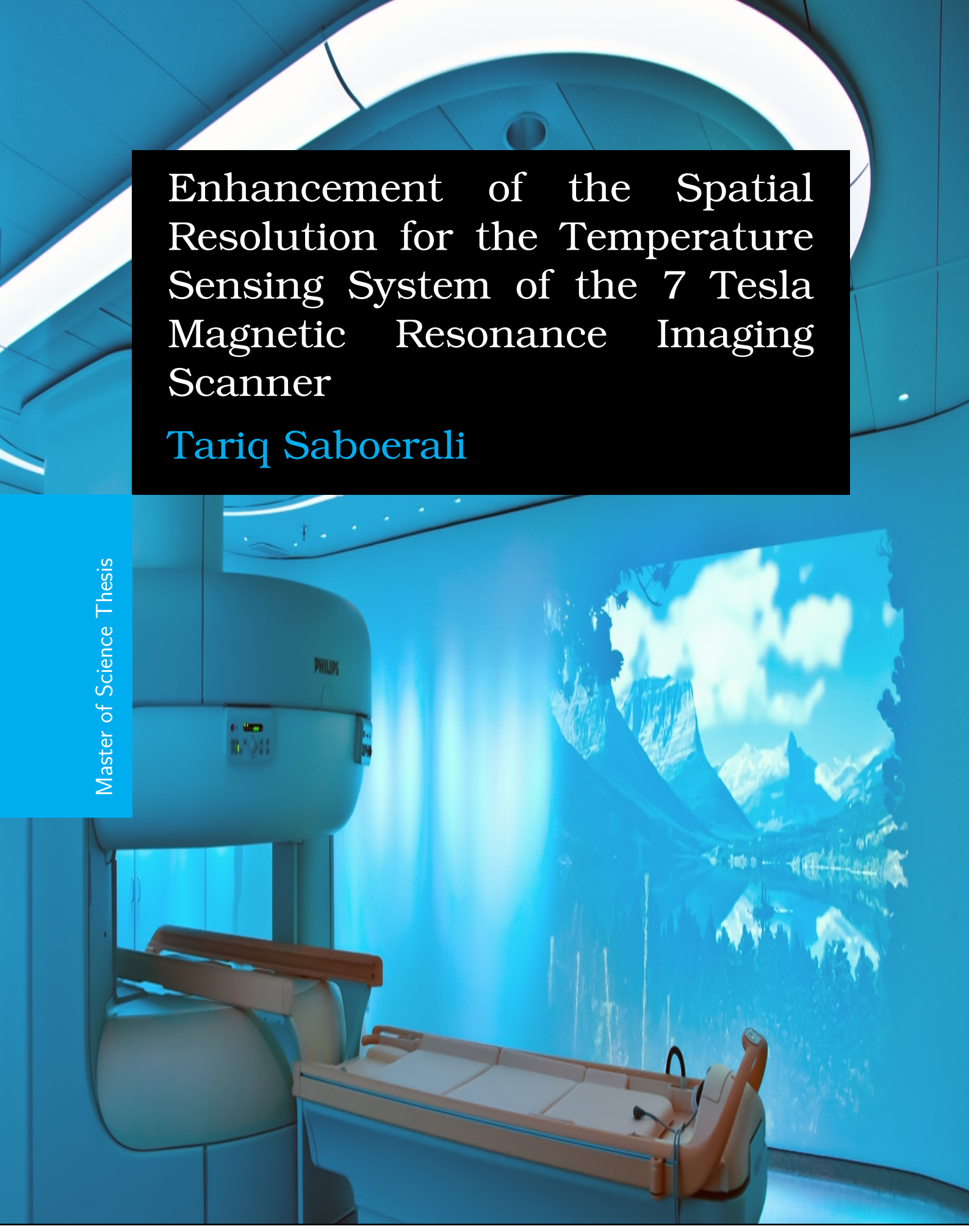

TU Delft Delft University of Technology

LUMC Leids Universitair Medisch Centrum

Enhancement of the Spatial Resolution for the Temperature Sensing System of the 7 Tesla Magnetic Resonance Imaging Scanner

Master of Science Thesis

In partial fulfillment of the requirements for the degree of Master of Science in Electrical Engineering at Delft University of Technology

Tariq Saboerali

January 20, 2017

Faculty of Electrical Engineering Mathematics and Computer Science (EEMCS)
Delft University of Technology

The work in this thesis was supported by the Leiden University Medical Centre. Their cooperation is hereby gratefully acknowledged.

Delft University of Technology
Department of
Circuits And Systems (cas)

Enhancement of the Spatial Resolution for the Temperature Sensing System of the 7 Tesla Magnetic Resonance Imaging Scanner

by

Tariq Saboerali

in partial fulfillment of the requirements for the degree of

Master of Science Electrical Engineering

January 20, 2017

Thesis committee members:

Prof. dr. ir. A.J. van der Veen	Professor of CAS Research group TU Delft
Dr. ir. Rob Remis	Assistant Professor CAS Research group TU Delft
Prof. Andrew Webb	Professor Gorter Center LUMC
Dr. ir. Rolf Hut	Postdoc Water Resources engineering TU Delft

Abstract

The MRI scanner with an ultrahigh magnetic field of 7T not only increases the image resolution but it also increases the Specific Absorption Rate (SAR) of the patient. In other words, the body temperature of the patient increases due to the absorption of heat produced by the 7T MRI scanner. This is dangerous for the health of the patient. In order to ensure that the SAR level of the patient does not exceed the acceptable limit, the body temperature of the patient should be monitored during the scan with a spatial resolution as small as possible. This way safety measures can be taken immediately if the body temperature increases. In order to monitor the temperature during the MRI scan, fiber optic sensors (FOS) can be used. The fiber optic sensors (FOS) are immune from electromagnetic interference and there is no electrical connection to the patient and thus it is safe to monitor the temperature during an MRI scan by using FOS [1]. However, the FOS may have a spatial resolution which is not acceptable for medical purposes. This study focuses on methods to increase the spatial resolution of an existing fiber optic temperature sensing system of a 7T MRI scanner. To increase the spatial resolution of the existing temperature sensing system two methods are evaluated, namely the total variation deconvolution method and the blind deconvolution method. This study shows that the total variation deconvolution method gives the best results for the input temperature estimate. The blind deconvolution method strongly depends on the initial guess of the impulse response of the temperature sensing system, which is difficult to find. Therefore the results of the input temperature and the impulse response are less reliable when using the blind deconvolution method. Also it is shown that the machine resolution gets worse when increasing the spatial resolution by interpolating the input temperature in the Fourier domain.

Table of Contents

List of Figures

List of Tables

Acknowledgements

During my last year at the Delft University of Technology I had the privilege to do a research project with the Leiden University Medical Center (LUMC). First of all, I would like to thank Dr. Rob Remis and Prof. Andrew Webb, who were both initiators of this thesis and my primary supervisors in the early stage, for giving me the opportunity to do this research. Many thanks to Dr. Rob Remis, from the Circuit and Systems section at the Delft University of Technology, for the scientific support and ideas. I also thank Dr. Rolf Hut of the civil engineering faculty for sharing his knowledge and ideas with me. Moving towards more personal acknowledgments, I would like to thank my parents, family and friends for constant support. Special thanks goes to my uncle and aunt, Jabbar Kurban and Badroen Kurban-Baboe, with whom I have lived for three years during my studies in the Netherlands. Without their support it would have been impossible for me to study in the Netherlands. Finally, I would like to acknowledge my co-students, that I have worked with over the two years while I was pursuing a Master degree at the faculty of Electrical Engineering Mathematics and Computer Science at the Delft University of Technology.

Delft, Tariq Saboerali
January 20, 2017

I would like to dedicate this thesis to my parents, Mr. Sherief Saboerali and Mrs. Amiroen Saboerali-Kurban, whom have supported me a lot during my studies at the Delft University of Technology.

> "The will to win, the desire to succeed, the urge to reach your full potential... these are the keys that will unlock the door to personal excellence."
>
> — *Confucius*

Chapter 1

Introduction

1-1 Magnetic Resonance Imaging

Today Magnetic Resonance Imaging (MRI) is being used in many hospitals worldwide as a diagnostic tool. The MRI technique uses strong magnetic fields and radio waves in order to produce anatomic images of the human body. This technique includes the use of protons, the positively charged and spinning nucleus of hydrogen atoms. Basically the concentration of protons is being imaged. In order to better understand the imaging process of MRI, a schematic view is drawn [2] and illustrated in (Figure 1-1).

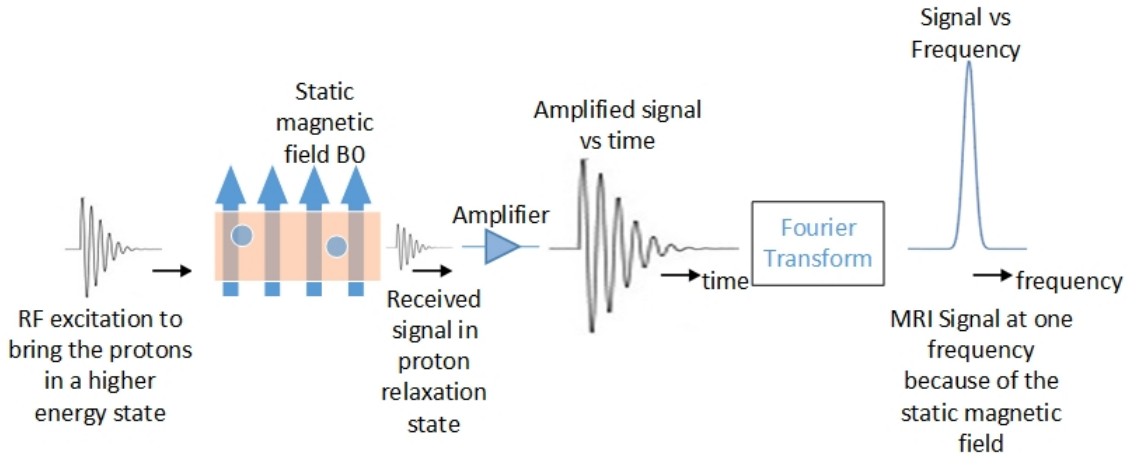

Figure 1-1: Schematic overview of Physical Principle MRI for static magnetic field

From Figure 1-1 it is observed that a static magnetic field is applied. The static magnetic field causes the protons in the body to align along that field. Protons can align either with or against the direction of the field. When the protons are excited by a radio frequency signal at the resonance frequency, the axes of the protons which were aligned with the magnetic field,

are momentarily aligned against the field in a high energy state. When the radio frequency field is turned off, energy is being released at the resonance frequency as the protons realign with the magnetic field. This process is called "relaxation." This released energy is being detected by the MRI sensors as a function of time, and then by using Fourier transformation it is converted to signal strength as a function of frequency. In Figure 1-1 the protons are subjected to the same magnetic field, hence they will produce the same radiation frequency and the Fourier transform of the detected signal has only one peak. This Fourier transformed signal demonstrates only the presence of protons, but no information about the location is given [2].

The location of the protons can be determined by adding a calibrated gradient magnetic field throughout the region of the whole sample as shown in Figure 1-2 [2].

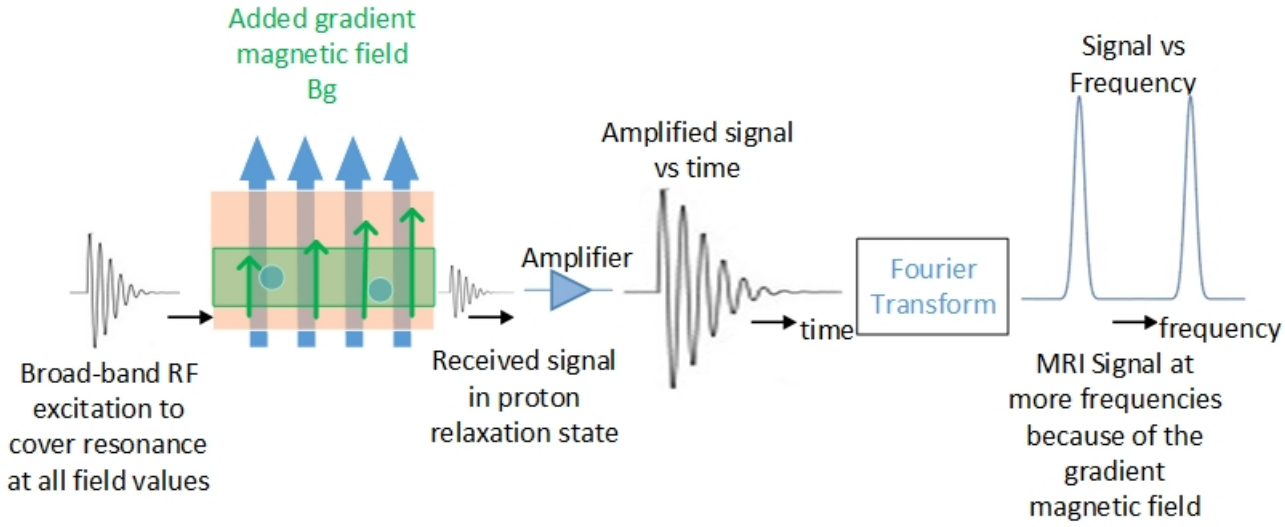

Figure 1-2: Schematic overview of Physical Principle MRI for gradient magnetic field

The magnetic field is increased across the sample from left to right and this leads to a frequency increase of the emitted signal from left to right. The protons are excited by an RF signal and thus will the emitted signal contain different frequencies for the two different proton concentration areas. The frequencies are separated by performing the Fourier transformation and the two different frequencies for the two different proton areas are given. In Figure 1-2 the protons are only located horizontally, there is no indication given about different heights.

In order to collect position information in different directions, a rotating field gradient is used. The position information from different directions is combined in order to produce a two-dimensional map of proton densities. The recorded signals are analyzed by computer algorithms and anatomic images are produced [2].

In MRI, the resolution of the image is an important aspect in order for a doctor to make reliable diagnostics. The resolution of the image depends on the magnetic field strength, tissue characteristics, density of protons, magnetic susceptibility and blood flow. Nowadays the 3T MRI scanner is already being used commercially, but the 7T MRI scanner is not commercially used yet. In this chapter we will briefly discuss the 3T and 7T MRI scanners [2].

1-2 Image Resolution 3T MRI

Today imaging is being performed by both the 1.5T and 3T MRI scanners. Advantage of the 3T MRI scanner compared to the 1.5T MRI scanner is that due to the increase of the spatial resolution and SNR (Signal to Noise Ratio) of the 3T scanner, higher quality images are produced. Although the SNR is proportional to the magnetic field, the SNR does not increase by a factor of two for 3T MRI compared to 1.5T MRI. The SNR increase is according to literature in the order of 1.5-1.7 and depends on several factors. The first major factor is that the relaxation time increases at a higher magnetic field strength which results in a decrease of the SNR. Furthermore the relaxation time increase rate depends on the tissue. For some tissue this increase is larger than for other tissues, therefore the SNR will decrease for some tissues and thus the resolution of the 3T MR image will be decreased. The second major factor is that the specific absorption rate (SAR) increases with the magnetic field strength increase. The SAR is the rate at which electromagnetic energy is absorbed by the human body when exposed to a radio frequency (RF) electromagneticfield. The patient safety needs to be guaranteed and thus additional actions needs to be taken when the SAR increases for 3T MRI compared to 1.5T MRI. These actions involve reduction of repetition time, decrease number of slices (number of spins in a plane through the object) and decrease of the flip angle. All these actions have a negative effect on MRI, because they increase scanning time, reduce contrast and further reduce the SNR when 3T MRI is compared to 1.5T MRI [3].

1-3 Image Resolution 7T MRI

The major advantage of using MRI with a higher static magnetic field is the increase of the Signal to Noise Ratio (SNR). This improves spatial and/or temporal resolution and reduces scan time while offering better image quality. MR Imaging at 7T is more challenging compared to 3T, because at 7T there is increased magnetic field inhomogeneities and higher SAR levels. The 7T MRI is not yet used for clinical diagnostics. At the moment, 7T is the strongest magnetic field possible in a human scanner [4].

Research on the 7T MRI is still going on. Although 7T provides a better and more detailed image than the 3T, it is not known at the moment if the 7T MRI can overcome the problems of the 3T MRI. In Figure 1-3, the MRI of the human brain is illustrated [4].

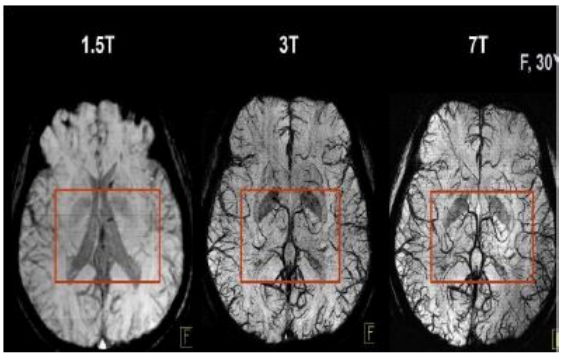

Figure 1-3: Detail difference between different scans

From this figure, the difference in detail between different MRIs with the use of static magnetic fields of 1.5T, 3T and 7T can be clearly observed. The 7T MRI is clearly more detailed than the 3T MRI and 1.5T MRI [4].

1-4 Temperature monitoring for 7T MRI with fiber optic sensors

From previous sections it is clear that by increasing the magnetic field strength, the image resolution becomes better but at the expense of a higher SAR level. If the SAR level gets too high, too much heat is absorbed by the human body and the body temperature may become prohibitively too high. This is one reason that the 7T MRI scanner is not commercially used yet. The Leiden University Medical Center (LUMC) wants to monitor the patient's temperature inside a 7T MRI scanner in order to be able to guarantee an acceptable SAR level. Moreover, the temperature needs to be measured with an acceptable spatial resolution and in a safe manner as well of course. To this end, fiber optic sensors (FOS) are used to measure the temperature.

In magnetic resonance imaging, FOS is ideal to use because it does not make any electrical connection to the patient and it is immune to electromagnetic interference. Other advantages of FOS in medical applications are: high accuracy, high sensitivity, makes distributed sensing possible, flexible, small size and light weight [6]. The FOS is in its basic form composed of a light source, an optical fiber, a sensing element and a detector. Figure 1-4 shows the working principle of FOS [6].

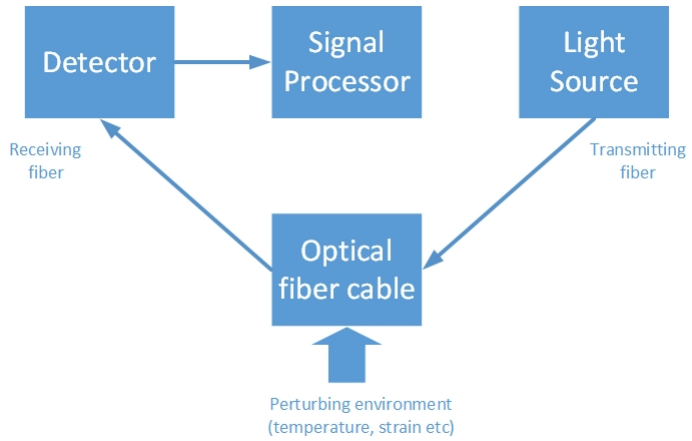

Figure 1-4: Basic working principle of FOS

The working principle of FOS is that the sensing element modulates some parameter of the optical system (intensity, wavelength, phase etc), which causes a change in the characteristics of the optical signal received at the detector. The key principle is that external physical parameters are measured by introducing changes in one or more optical properties of a light beam traveling inside an optical fiber. The optical fiber is thus both the sensing element and transmission medium.

With FOS it is possible to measure many physical properties like light intensity, displacement, temperature, pressure rotation, sound, strain,magnetic field, electric field, radiation, flow, liquid level, chemical analysis, and vibration [6].

1-5 Problem definition

1-5-1 Objective

The LUMC can already measure the temperature of the patient inside a 7T MRI scanner, but with a spatial resolution of 12.5cm. This spatial resolution is not sufficient and needs to be improved. The temperature measurements are performed with a distributed temperature sensing system which makes use of fiber optic sensors based on Raman spectroscopy. The objective of this thesis is to accurately estimate the input temperature and to improve the spatial resolution of the current temperature sensing system during a 7T MRI scan. By improving the spatial resolution and temperature readings accuracy, the temperature of the patient inside a 7T MRI scanner can be measured more accurately and therefore it will be better known what amount of heat (produced by the 7T MRI scanner) should be suppressed in order to guarantee safe SAR levels for the patient.

1-5-2 Research question

What method can be used to improve the spatial resolution of the temperature sensing system for a 7T MRI scanner at the LUMC?

1-5-3 Sub questions

- From literature it is known that with a total variation deconvolution algorithm the input temperature can be estimated more accurate and by Fourier domain interpolation the spatial resolution of the input temperature can be increased. Can the spatial resolution be improved to an acceptable level with the total variation deconvolution algorithm?
- With a blind deconvolution algorithm the input temperature can be estimated and by Fourier domain interpolation the spatial resolution of the input temperature can be increased. Can the blind deconvolution algorithm give an accurate temperature reading with an increased spatial resolution?

1-6 Thesis outline

Chapter 2 describes the theoretical framework on fiber optic sensors. In section 2.1.1 the theoretical background of fiber optic sensors is described which makes use of fiber Bragg grating. In section 2.1.2 the theoretical background of fiber optic sensors is described which makes use of Raman spectroscopy. In section 2.2 the increase of the spatial resolution is described based on a total variation deconvolution algorithm. Section 2.3 describes the impulse response estimation and the blind deconvolution algorithm. Chapter 3 describes the results. In section 3.1 the results of the impulse response estimate are discussed by using different methods, section 3.2 describes the input temperature estimation by using two different algorithms and finally section 3.3 describes the spatial resolution increase by using Fourier domain interpolation. Finally chapter 4 provides conclusions and discussions and future research work is discussed in chapter 5.

Chapter 2

Theoretical Framework

The temperature sensing system which is used for the 7T MRI at LUMC, consists of fiber optic sensors and makes use of Raman spectroscopy. In this chapter we start with a discussion on fiber optic sensors. After this it is described how the spatial resolution of the fiber optic sensors can be improved in order to monitor the body temperature of the patient with an acceptable spatial resolution.

2-1 Working Principle of Fiber Optic Sensors

2-1-1 Fiber Bragg grating technique

Temperature variations can be measured by FOS which make use of Fiber Bragg Grating (FBG) technology or Raman spectroscopy. In this subsection the FBG technology will be discussed and in the next subsection Raman spectroscopy will be discussed.

The FBG technology is based on reflection of radiation which is caused by a Bragg grating. Bragg grating is when in fiber optic with FBG only a narrow range of wavelengths are reflected. The reflected wavelength (λ), also called the Bragg wavelength is defined as

$$\lambda_B = 2 \times \Lambda \times \eta_{eff}. \tag{2-1}$$

In Eq. (2-1), η_{eff} is the effective refraction index of the core of the fiber optic cable and Λ is the spatial period of the grating. The influence of temperature on the effective refraction index and on the grating spatial period, makes it possible to measure the temperature with FOS.

The change in temperature causes a shift in the Bragg wavelength. This occurs due to thermal expansion which changes the grating spacing and the effective refraction index also changes with temperature. The Bragg wavelength shift $\Delta\lambda_B$ is given by

$$\Delta\lambda_B = \lambda_B(\alpha + \zeta)\Delta T. \tag{2-2}$$

In Eq. (2-2), α is equal to the thermal expansion coefficient for fiber and ζ is equal to the thermo-optic coefficient for fiber. The temperature change is equal to ΔT. By measuring the change of the spatial period of grating and refraction index, the shift in Bragg wavelength can be calculated. From this shift the temperature can be calculated [7].

The purpose of this project is to monitor the body temperature of a patient inside the 7T MRI scanner. Hence the temperature needs to be monitored on different points of the body with a spatial resolution of less than 12.5cm. Thus the position also needs to be determined along with the body temperature. This can be achieved by using a linearly chirped fiber bragg grating (LCFBG) sensor which uses a linearly frequency modulated (chirped) optical waveform (LFMOW). The LFMOW can be generated with a laser diode (LD) through linear frequency modulation, which can be realized by feeding a sawtooth current into the LD. This generated LFMOW can then be sent to a pair of LCFBG sensors with one serving as a sensing LCFBG and the other as a reference LCFBG. Both LCFBG sensors will cause a reflection of the LFMOW signal and this results in the generation of two time-delayed LFMOWs. From the time delay difference between the two LFMOWs, the range can be calculated, hence the exact position in the optical fiber can be estimated which corresponds with a certain temperature. In Figure 2-1 the schematic overview of FBG is provided. The time delay difference (τ) is calculated according to

$$\tau = \frac{2nL}{c}. \tag{2-3}$$

In Eq. (2-3), L is equal to the distance between the two LCFBGs, n is the refractive index of the fiber and c is equal to the speed of light in vacuum [8]. When τ is known then the range R (position in the optical fiber) can be calculated as

$$R = \frac{c\tau}{2}. \tag{2-4}$$

The LFMOW signals are fed into a photo detector (PD), which produces a microwave beat signal with a frequency that is proportional to the time delay difference between the two reflected waveforms. The sensing LCFBG will react on the temperature and this results in a shift of the spectral response of the sensing LCFBG. This leads to the change of the beat frequency. By measuring the beat frequency, the time delay can be estimated, which is used to estimate the Bragg wavelength shift and thus the temperature can also be estimated.

Now will be described how the temperature depends on the beat frequency. First the instantaneous optical frequency $\omega_1(t)$ is defined as

$$\omega_1(t) = \omega_0 + \beta t. \tag{2-5}$$

Here ω_0 is equal to the angular frequency at the start of a period of the LFMOW signal and β is equal to the chirp rate of the reference LCFBG. In this equation, β is equal to $2\pi\Delta f/T_S$, where Δf is equal to the frequency deviation and T_S is the period of the waveform. The electric field of the reference signal is given by

$$E_1(t) = A_1 \exp[j(\omega_0 t + \frac{1}{2}\beta t^2 + \phi_0)]. \tag{2-6}$$

In Eq. (2-6), A_1 is equal to the amplitude of the signal and ϕ_0 is equal to the phase of the signal. The angular frequency of the time-delayed sensing signal is given by

$$\omega_2(t) = \omega_0 + \beta(t - \tau), \tag{2-7}$$

and the electric field of the time-delayed sensing signal is given by

$$E_2(t) = A_2 \exp\{j[\omega_0(t-\tau) + \frac{1}{2}\beta(t-\tau)^2 + \phi_0]\}. \tag{2-8}$$

Both the reference signal and sensing signal need to be fed into a photodetector which generates a beat signal. This beat signal is [8]

$$\begin{aligned} s(i,\tau) &= |E_1(t) + E_2(t,\tau)|^2 \\ &= [|E_1(t) + E_2(t,\tau)|][|E_1(t) + E_2(t,\tau)|]^* \\ &= E_1(t)E_1(t)^* + E_2(t,\tau)E_2(t,\tau)^* \\ &+ E_1(t)E_2(t,\tau)^* + E_1(t)^*E_2(t,\tau). \end{aligned}$$

The expression of the beat signal is further worked out and the electric field of the reference signal is

$$E_1(t) = A_1[\cos(\omega_0 t + \frac{1}{2}\beta t^2 + \phi_0) + j\sin((\omega_0 t + \frac{1}{2}\beta t^2 + \phi_0)],$$

and by multiplying the reference electric field with its complex conjugate we get

$$\begin{aligned} E_1(t)E_1(t)^* &= A_1[\cos(\omega_0 t + \frac{1}{2}\beta t^2 + \phi_0) + j\sin((\omega_0 t + \frac{1}{2}\beta t^2 + \phi_0)] \\ &* A_1[\cos(\omega_0 t + \frac{1}{2}\beta t^2 + \phi_0) - j\sin((\omega_0 t + \frac{1}{2}\beta t^2 + \phi_0)] \\ &= A_1^2 = I_1. \end{aligned}$$

The electric field of the sensing signal is

$$\begin{aligned} E_2(t,\tau) = A_2[&\cos(\omega_0(t-\tau) + \frac{1}{2}\beta(t-\tau)^2 + \phi_0) \\ &+ j\sin(\omega_0(t-\tau) + \frac{1}{2}\beta(t-\tau)^2 + \phi_0)], \end{aligned}$$

and by multiplying the sensing electric field with its complex conjugate we get

$$\begin{aligned} E_2(t,\tau)E_2(t,\tau)^* &= A_2[\cos(\omega_0(t-\tau) + \frac{1}{2}\beta(t-\tau)^2 + \phi_0) + j\sin(\omega_0(t-\tau) + \frac{1}{2}\beta(t-\tau)^2 + \phi_0)] \\ &* A_2[\cos(\omega_0(t-\tau) + \frac{1}{2}\beta(t-\tau)_2 + \phi_0) - j\sin(\omega_0(t-\tau) + \frac{1}{2}\beta(t-\tau)^2 + \phi_0)] \\ &= A_2^2 = I_2. \end{aligned}$$

The summation of the third and fourth term of the beat signal expression gives

$$\begin{aligned} E_1(t)E_2(t,\tau)^* + E_1(t)^*E_2(t,\tau) &= 2A_1A_2\cos(\omega_0 t + \frac{1}{2}\beta t^2 + \phi_0)\cos(\omega_0(t-\tau) + \frac{1}{2}\beta(t-\tau)^2 + \phi_0) \\ &+ 2A_1A_2\sin(\omega_0 t + \frac{1}{2}\beta t^2 + \phi_0)\sin(\omega_0(t-\tau) + \frac{1}{2}\beta(t-\tau)^2 + \phi_0) \\ &= 2A_1A_2\cos[(\omega_0 t + \frac{1}{2}\beta t^2 + \phi_0) - (\omega_0(t-\tau) + \frac{1}{2}\beta(t-\tau)^2 + \phi_0)] \\ &= 2A_1A_2\cos(\beta\tau t + \omega_0\tau - \frac{1}{2}\beta\tau^2) \\ &= 2\sqrt{I_1I_2}\cos(\beta\tau t + \omega_0\tau - \frac{1}{2}\beta\tau^2), \end{aligned}$$

hence, the beat signal is

$$\begin{aligned} &E_1(t)E_1(t)^* + E_2(t,\tau)E_2(t,\tau)^* \\ &+ E_1(t)E_2(t,\tau)^* + E_1(t)^*E_2(t,\tau) \\ &= I_1 + I_2 + 2\sqrt{I_1 I_2}\cos(\beta\tau t + \omega_0\tau - \frac{1}{2}\beta\tau^2). \end{aligned}$$

The beat signal is thus

$$s(i,\tau) = I_1 + I_2 + 2\sqrt{I_1 I_2}\cos(\beta\tau t + \omega_0\tau - \frac{1}{2}\beta\tau^2). \tag{2-9}$$

In Eq. (2-9), I_1 and I_2 are equal to respectively the intensities of the reference and sensing signals. In Eq. (2-9), the term $\frac{1}{2}\beta t^2$ can be neglected because this term is close to zero. Therefore the frequency of the beat signal (f_b) is

$$f_b = \frac{\beta\tau}{2\pi}. \tag{2-10}$$

From Eq. (2-10) we conclude that the beat frequency depends on the time delay, which means that for every distance the beat frequency will change, because the time-delay changes over distance. So every point will have another beat frequency and by monitoring the beat frequency the temperature can be determined for every point on the human body. By monitoring the time delay, the range (distance that the signal traveled from a point on the human body towards the LCFBG) can be calculated as discussed earlier, and so the position can be determined that is related to a certain temperature in a point on the human body. The spatial resolution can be reduced by decreasing the time delay. The Bragg wavelength shift leads to a shift in beat frequency. Earlier it is mentioned that from the Bragg wavelength shift, the temperature can be measured (see Eq. (2-2)). From literature it is found that the relation between beat frequency shift and temperature is given by [8]

$$\Delta f_b = \frac{\beta}{2\pi} \times \frac{2\eta\lambda_B}{cC_{\text{chirp}}}(\alpha + \zeta)\Delta T. \tag{2-11}$$

In Eq. (2-11), C_{chirp} is the chirp rate of the sensing LCFBG. By measuring the shift in beat frequency, the temperature can be calculated.

In Figure 2-1 [8] it is shown that an LFMOW signal is generated by feeding a sawtooth current (from the signal generator) into a laser diode controller. The generated LFMOW signal is sent to a pair of LCFBG sensors through a distributed feedback laser diode (DFB LD). One LCFBG is serving as a sensing LCFBG and the other as a reference LCFBG. Both LCFBG will cause a reflection of the LFMOW signal and this results in the generation of two time-delayed LFMOWs. The reflected LFMOWs are sent to a photodetector through an optical circulator. The output of the photodetector is sent to a spectrum analyzer. From the time-delayed LFMOWs the beat frequency vs range can be shown on the spectrum analyzer. From the beat frequency shift the temperature can be calculated.

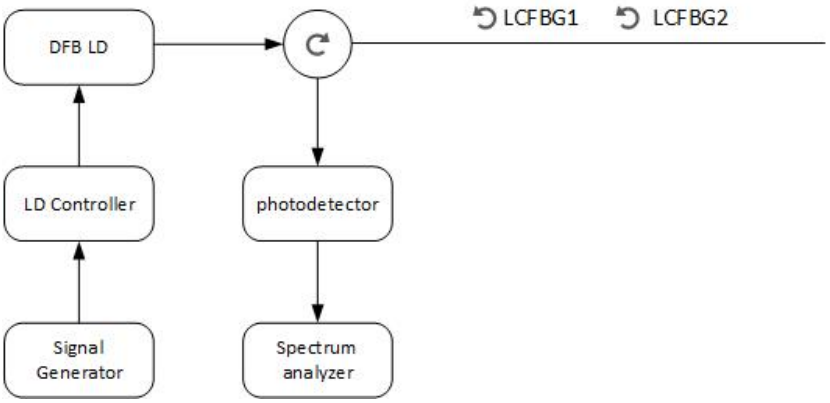

Figure 2-1: Schematic overview of FBG

So far the temperature sensing based on fiber Bragg grating is discussed. Another method which can be used to measure the temperature as a function of distance is based on Raman spectroscopy.

2-1-2 Raman spectroscopy

The Raman spectroscopy distributed temperature sensing method is a good method to measure the temperature because it has been proven [6] that the anti-Stokes Raman scattering component is highly temperature sensitive. The Raman Distributed Temperature Sensing (DTS) method is based on the ratio of the Stokes to anti-Stokes backscattering intensity as a function of time. Thus, with this method not only the temperature is measured but also the distance (because of the time dependency) in the fiber optic cable. In literature [6] the Raman scattering intensity I_R is given by

$$I_R = \frac{I_0 N_0 \sigma_R}{(\lambda_i \pm \lambda)^4}. \tag{2-12}$$

In Eq. (2-12), I_0 is equal to the intensity of the incident signal, λ_i is the wavelength of the incident signal and σ_R is the Raman cross section. The Stokes intensity is given by [6]

$$I_S = \frac{I_0 N_g \sigma_R}{(\lambda_i + \lambda)^4}, \tag{2-13}$$

and the anti-Stokes intensity is [6]

$$I_{AS} = \frac{I_0 N_g e^{v/kT} \sigma_R}{(\lambda_i - \lambda)^4}. \tag{2-14}$$

In Eq. (2-14), v is equal to the spatial frequency of the wave, k is the Boltzmann constant, and T is the temperature. The anti-Stokes component is dependent on the absorption of energy from photons. This energy absorption depends on the temperature and thus this dependency makes the anti-Stokes component sensitive to temperature.

The Stokes to anti-Stokes ratio is given by [6]

$$R(T) = \frac{I_{AS}}{I_S} = \left(\frac{\lambda_S}{\lambda_{AS}}\right)^4 e^{-hc\Delta v/kT}. \tag{2-15}$$

In Eq. (2-15), λ_S is equal to the Stokes wavelength, λ_{AS} is equal to the anti-Stokes wavelength, h is the Planck constant, T is the absolute temperature of the fiber core under measurement, c is the speed of light in vacuum and Δv is the difference in spatial frequency between the incident wave and scattered wave. The absolute temperature is determined by locating a reference fiber coil in a controlled temperature bath. This coil is maintained at a known temperature θ. This produces a backscatter ratio $R(\theta)$. The unknown temperature T can then be determined along the arbitrary section of the sensing fiber by rearranging Eq. (2-15) and this is done as follows

$$T = \frac{R(T)}{R(\theta)},$$

working this out gives

$$T = \frac{\left(\frac{\lambda_S}{\lambda_{AS}}\right)^4 e^{-hc\Delta v/kT}}{\left(\frac{\lambda_S}{\lambda_{AS}}\right)^4 e^{-hc\Delta v/k\theta}} = \frac{e^{-hc\Delta v/kT}}{e^{-hc\Delta v/k\theta}},$$

and by taking the natural logarithm of the numerator and the denominator we get

$$\ln\left(\frac{R(T)}{R(\theta)}\right) = \ln\left(\frac{e^{-hc\Delta v/kT}}{e^{-hc\Delta v/k\theta}}\right) = \frac{-hcv}{kT} + \frac{hcv}{k\theta},$$

which is equal to

$$\frac{-hcvk\theta}{kTk\theta} + \frac{hcvkT}{k\theta kT} = \frac{k(-hcv\theta + hcvT)}{k(Tk\theta)},$$

and thus,

$$\ln\left(\frac{R(T)}{R(\theta)}\right) = \frac{k(-hcv\theta + hcvT)}{k(Tk\theta)}.$$

We further simplify this last equation by multiplying both sides of the equation with $Tk\theta$ and we get

$$Tk\theta \ln\left(\frac{R(T)}{R(\theta)}\right) = -hcv\theta + hcvT.$$

Solving this equation gives

$$Tk\theta \ln\left(\frac{R(T)}{R(\theta)}\right) - hcvT = -hcv\theta,$$

and the temperature is given by

$$T = \frac{-hcv\theta}{k\theta \ln\left(\frac{R(T)}{R(\theta)}\right) - hcv}.$$

By taking the inverse of the temperature we get

$$\frac{1}{T} = \frac{k\theta \ln\left(\frac{R(T)}{R(\theta)}\right) - hcv}{-hcv\theta} = \frac{1}{\theta} - \frac{k}{hcv} \ln\left(\frac{R(T)}{R(\theta)}\right),$$

and finally the temperature (T) is

$$T = \left[\frac{1}{\theta} - \frac{k}{hcv} \ln\left(\frac{R(T)}{R(\theta)}\right)\right]^{-1}. \tag{2-16}$$

Thus, to determine the temperature, the backscatter ratios $R(T)$ and $R(\theta)$ need to be measured. The backscatter ratio $R(T)$ is measured at the arbitrary section of the fiber and $R(\theta)$ is measured at the reference fiber coil. The location on the human body where the temperature is measured is calculated using the optical time domain reflectometer (OTDR) principle. The OTDR injects a train of pulses in the optical fiber under test and calculates the travel time of each pulse that is reflected back. From the travel time the distance is calculated. Hence the temperature can be measured as a function of distance. To reduce the spatial resolution, the travel time of the pulses needs to be minimized. This can be achieved by injecting a train of pulses with a high pulse repetition frequency (PRF). The distance is calculated as

$$R = \frac{ct}{2}. \tag{2-17}$$

In Eq. (2-17), R is equal to the distance that the pulse travels in the fiber optic cable, c is the speed of light in vacuum and t is the travel time of the pulse.

Figure 2-2 [6] illustrates the simple operating principle of the Raman DTS. From this figure it is observed that a laser injects light pulses into the optical fiber. This incident light pulse is reflected back and from the reflected light pulse (as discussed above) the temperature is measured by the detector. From the time delay between the incident and reflected pulse, the distance is calculated (as discussed earlier).

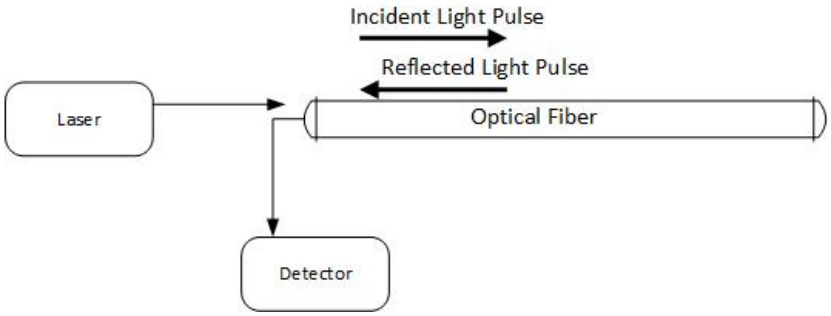

Figure 2-2: Schematic overview of Raman scattering DTS

Figure 2-3 shows the used test formation of the temperature measurement with Raman spectroscopy. The fiber optic cable goes from the DTS (Distributed Temperature Sensing system) to an ice bath (for calibration) and then it goes to the hot object to measure the temperature and after that it goes again in an ice bath for calibration.

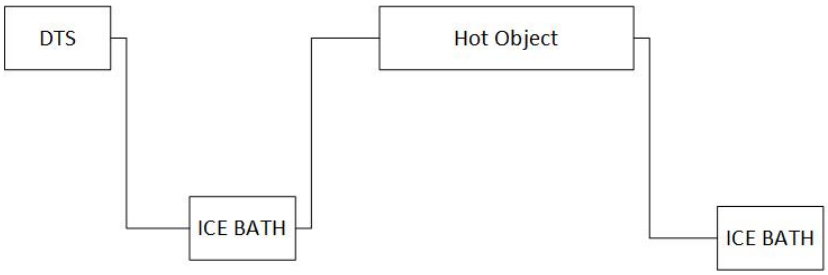

Figure 2-3: Schematic overview of test formation

In this paragraph two methods have been discussed to measure the temperature of the human body inside the 7T MRI scanner. These two methods are the fiber grating method and the Raman spectroscopy method. From the fiber grating method we have seen that in this case two LCFBG sensors are needed. For the Raman spectroscopy method only the $R(T)$ and $R(\theta)$ need to be measured. Also only one train of pulses is injected into the fiber from which we can calculate the distance. This makes the Raman spectroscopy method less complex compared to the FBG method. It also may be the case that the FBG method will be more expensive to use in practice, because of its higher complexity. Therefore the LUMC uses the Raman spectroscopy method.

2-2 Increase of the spatial resolution of Fiber Optic Sensors

In this thesis the spatial resolution is defined as the distance between each sample point. In order to increase the spatial resolution of the DTS, the distance between the sample points should be decreased hence temperature should be measured at more points on the human body.

In [9] it is shown that the spatial resolution of a distributed optical fiber temperature sensing system can be increased by the use of superconducting nanowire single-photon detectors and single-photon counting techniques. In [9] it is shown that the uncertainty of temperature measurements decreases with increasing integration periods. The temperature uncertainty is in the order of 3 Kelvin with a spatial resolution of 1cm and an integration period of 60 seconds. However this technique has a high cost and also the increase in spatial resolution leads to an increase in measurement uncertainty and response time. Due to these complications it should not be used for medical purposes. Therefore in this thesis it is proposed to use a signal processing technique which increases the spatial resolution of the measurement without increasing equipment costs, because no physical changes in the device are required. The signal processing techniques which are proposed are the total variation deconvolution method and the blind deconvolution method.

The output of the distributed temperature sensing (DTS) system can modeled as a convolution between the real temperature profile (input) and the impulse response of the DTS system. It is considered that the DTS is a Linear Time Invariant (LTI) system [10] and it is modeled as

$$r(z) = p(z) * t(z). \tag{2-18}$$

In Eq. (2-18), z is the distance (in cm) along the fiber optic cable, p is the impulse response of the DTS system, r is the temperature reading of the DTS and t is the real temperature profile. The model from Eq. (2-18) is discretized and rewritten in matrix vector notation as

$$\mathbf{r} = \mathbf{P}\mathbf{t} + \mathbf{n}. \tag{2-19}$$

In Eq. (2-19), $\mathbf{r}$ is equal to the DTS temperature reading, $\mathbf{P}$ is the sensitivity matrix which is constructed from the DTS impulse response, $\mathbf{t}$ is the real temperature profile and $\mathbf{n}$ is additive white Gaussian noise (AWGN). Due to the ill-conditioning of matrix $\mathbf{P}$, a simple inversion of Eq. (2-19) in order to obtain the temperature profile $\mathbf{t}$ will result in high noise amplification and large errors between the estimated value of $\mathbf{t}$ and exact value of $\mathbf{t}$. The error needs to be minimized by using a least squares method. This problem is a regularization problem and as an approximate solution we take [10]

$$\hat{\mathbf{t}} = \text{argmin}||\mathbf{r} - \mathbf{P}\mathbf{t}||_2^2 + \lambda||\mathbf{D}\mathbf{t}||_1. \tag{2-20}$$

In Eq. (2-20), $\hat{\mathbf{t}}$ is equal to the reconstructed temperature profile, λ is the regularization parameter which controls the sensitivity to noise, and $\mathbf{D}$ is a finite difference matrix. The linear least squares error is minimized by setting the gradient of $\hat{\mathbf{t}}$ to zero. In Eq. (2-20), $\mathbf{t}$ is a vector which consists of temperatures on each measured point, that is

$$\mathbf{t} = \begin{pmatrix} t_1 \\ t_2 \\ \vdots \\ t_N \end{pmatrix},$$

and the differentiation matrix is given by

$$\mathbf{D} = \frac{1}{\Delta} \begin{bmatrix} -1 & 1 & 0 & \dots & & \\ 0 & -1 & 1 & \dots & & \\ \vdots & \vdots & -1 & 1 & & \\ \vdots & \vdots & \vdots & \ddots & \ddots & \\ \dots & \dots & \dots & \dots & -1 & 1 \end{bmatrix},$$

and thus is $||\mathbf{D}\mathbf{t}||_1$ given by

$$||\mathbf{D}\mathbf{t}||_1 = \frac{\sum_{i=1}^{n-1} |t_{i+1} - t_i|}{\Delta},$$

where Δ is the difference in distance between two temperature measurements. Eq. (2-20) is solved with the Iterative Re-weighted Least Squares (IRLS) method and the solution is updated by solving a least squares problem and reiterated until a minimum specified error is obtained.

The total variation deconvolution algorithm provides an accurate estimate of the real input temperature. This is important to know for medical purposes because the reading errors due to noise can result in a poor DTS output which may endanger the health of the patient. After the input temperature profile is constructed, interpolation in Fourier domain is used to increase the spatial resolution of the DTS.

At points where the difference in temperature ($\mathbf{Dt}$) is zero the L1 norm of the absolute values of $\mathbf{Dt}$ become non-differentiable and thus $\hat{\mathbf{t}}$ is not differentiable at these points. At points where the difference in temperature ($\mathbf{Dt}$) is non-zero, the gradient of $\hat{\mathbf{t}}$ can be calculated. The gradient of $\hat{\mathbf{t}}$ is determined as follows [10]

$$\frac{\delta}{\delta \mathbf{t}}||\mathbf{r}-\mathbf{Pt}||_2^2 = -2\mathbf{P}^T(\mathbf{r}-\mathbf{Pt}),$$

we simplify $||\mathbf{Dt}||_1$ and we get

$$||\mathbf{Dt}||_1 = \frac{\sum_{i=1}^{n-1}|t_{i+1}-t_i|}{\Delta} = \frac{\sum_{i=1}^{n-1}|\gamma_i|}{\Delta},$$

and differentiating this with respect to $\mathbf{t}$ gives

$$\frac{\delta|\mathbf{Dt}|_1}{\delta \mathbf{t}_k} = \frac{\delta|\gamma_i|}{\delta \mathbf{t}_k} = \sum_{i=1}^{n-1} D_{i,k}\frac{\gamma_i}{|\gamma_i|}.$$

The diagonal matrix $\mathbf{W}$ is defined with elements, $W_{i,i} = \frac{1}{|\gamma_i|}$ and thus, the gradient of $\nabla(||\mathbf{Dt}||_1)$ is

$$\nabla(||\mathbf{Dt}||_1) = \mathbf{D}^T\mathbf{WDt},$$

and finally the gradient of $\hat{\mathbf{t}}$ is

$$\nabla\hat{\mathbf{t}} = -2\mathbf{P}^T(\mathbf{r}-\mathbf{Pt}) + \lambda\mathbf{D}^T\mathbf{WDt}. \tag{2-21}$$

To minimize the linear least squares error, the gradient of $\hat{\mathbf{t}}$ is set to zero, and thus we get

$$2\mathbf{P}^T\mathbf{r} = 2\mathbf{P}^T\mathbf{Pt} + \lambda\mathbf{D}^T\mathbf{WDt} = (2\mathbf{P}^T\mathbf{P} + \lambda\mathbf{D}^T\mathbf{WD})\mathbf{t}, \tag{2-22}$$

from which the input temperature follows

$$\hat{\mathbf{t}} = 2\mathbf{P}^T\mathbf{r}(2\mathbf{P}^T\mathbf{P} + \lambda\mathbf{D}^T\mathbf{WD})^{-1}. \tag{2-23}$$

Note that $\mathbf{W}$ is not defined where $\mathbf{Dt}$ is zero. In order to cope with the non-differentiability of the 1-norm, a tolerance ϵ is set and $W_{i,i}$ is [10]:

$$W_{i,i} = \frac{1}{|\gamma_i|} \quad \text{if} \quad |\gamma_i| \geq \epsilon \quad ; \quad W_{i,i} = \frac{1}{\epsilon} \quad \text{if} \quad |\gamma_i| < \epsilon \tag{2-24}$$

Eq. (2-20) is solved by the IRLS procedure where $\mathbf{W}$ is updated according to Eq. (2-24) and these steps are repeated until the solution converges.

In order to implement the total variation deconvolution, the impulse response of the DTS need first to be estimated. In the next section two methods (including the blind deconvolution method) are discussed in order to estimate this impulse response.

2-3 Impulse response estimation

The only information which is known, is the DTS temperature reading. Hence $\mathbf{t}$ and $\mathbf{p}$ are unknown and need to be estimated. In this section two methods are discussed in order to estimate the impulse response:

1. The input $\mathbf{t}$ is assumed to be ideal and $\mathbf{p}$ is estimated with the total variation deconvolution method.
2. Both $\mathbf{t}$ and $\mathbf{p}$ are unknown and therefore estimated with the blind deconvolution method.

2-3-1 Ideal input

The input of the DTS is assumed ideal and $\mathbf{p}$ is estimated with the Maximum Likelihood Estimation (MLE) method. The output of the DTS is calculated as the convolution between the impulse response of the DTS and the input, that is

$$r(z) = p(z) * t(z) + n(z). \tag{2-25}$$

In Eq. (2-25), r signifies the DTS reading, p is the impulse response, t is the input temperature and n is noise. The DTS reading is a function of distance z.

In discrete form, the convolution between the impulse response and temperature is

$$r(n) = \sum_{k=0}^{m-1} p_k t_{n-k} \Delta z + n_n \quad \text{with} \quad n = m-1, ..., N-1.$$

Writing this out gives

$$\begin{pmatrix} r_{m-1} \\ r_m \\ r_{m+1} \\ \vdots \\ r_{N-1} \end{pmatrix} = \Delta z \begin{bmatrix} t_{m-1} & t_{m-2} & t_{m-3} & \dots & t_0 \\ t_m & t_{m-1} & t_{m-2} & \dots & t_1 \\ t_{m+1} & t_m & t_{m-1} & \dots & t_2 \\ \vdots & \vdots & \vdots & \ddots & \vdots \\ \vdots & \vdots & \vdots & \ddots & \vdots \\ t_{N-1} & t_{N-2} & t_{N-3} & \dots & t_{N-m} \end{bmatrix} \begin{pmatrix} p_0 \\ p_1 \\ p_2 \\ \vdots \\ p_{m-1} \end{pmatrix} + \begin{pmatrix} n_{m-1} \\ n_m \\ n_{m+1} \\ \vdots \\ n_{N-1} \end{pmatrix},$$

and in matrix-vector form this becomes

$$\mathbf{r} = \mathbf{T}\mathbf{p} + \mathbf{n}. \tag{2-26}$$

The following assumptions are made:

1. Observations are independent and have random errors which are normally distributed with zero mean.
2. The noise is modeled as white Gaussian noise with zero mean and variance C.

The joint probability density function for independent observations of $\mathbf{r}$ is

$$t(\mathbf{r}|\mathbf{p}) = t_1(r_1|\mathbf{p}).t_2(r_2|\mathbf{p})....t_m(r_m|\mathbf{p}). \tag{2-27}$$

The likelihood function L is the probability of $\mathbf{p}$ given an observed $\mathbf{r}$ which is equal to

$$L(\mathbf{p}|\mathbf{r}) = t(\mathbf{r}|\mathbf{p}), \tag{2-28}$$

and $\mathbf{p}$ is estimated by maximizing the likelihood function L. This is called Maximum Likelihood Estimation (MLE). Taking the above mentioned assumptions into account, the joint probability density function of one sample is

$$t_i(r_i|\mathbf{p}) = \frac{1}{\sigma_i\sqrt{2\pi}} e^{-\frac{1}{2}(r_i-(\mathbf{Tp})_i)^2/\sigma_i^2}. \tag{2-29}$$

The likelihood function L for the complete data set is the product of the individual likelihoods and is equal to

$$L(\mathbf{p}|\mathbf{r}) = \frac{1}{(2\pi)^{m/2}\prod_{i=1}^{m}\sigma_i} \prod_{i=1}^{m} e^{-\frac{1}{2}(r_i-(\mathbf{Tp})_i)^2/\sigma_i^2}. \tag{2-30}$$

The term: $\frac{1}{(2\pi)^{m/2}\prod_{i=1}^{m}\sigma_i}$ has no effect on the maximization so we maximize L and therefore we look for a $\mathbf{p}$ such that

$$\max \prod_{i=1}^{m} e^{-\frac{1}{2}(r_i-(\mathbf{Tp})_i)^2/\sigma_i^2}. \tag{2-31}$$

In equation Eq. (2-31), we take the logarithm and then we get

$$\max \left[-\frac{1}{2} \sum_{i=1}^{m} \frac{(r_i - (\mathbf{Tp})_i)^2}{\sigma_i^2} \right]. \tag{2-32}$$

In order to maximize Eq. (2-31) we have to solve

$$\min \left[\sum_{i=1}^{m} \frac{(r_i - (\mathbf{Tp})_i)^2}{\sigma_i^2} \right]. \tag{2-33}$$

To solve this minimization problem, we take the derivative of the term inside the summation of Eq. (2-33) with respect to $\mathbf{p}$ and set this to zero. In other words we need to solve

$$\frac{\delta}{\delta \mathbf{p}}\left(\frac{(r_i-(\mathbf{Tp})_i)^2}{\sigma_i^2}\right)=0. \tag{2-34}$$

By solving Eq. (2-34) we obtain the MLE of $\mathbf{p}$ and that is

$$\hat{\mathbf{p}}_{\mathrm{MLE}}=\frac{\mathbf{r}\mathbf{T}^T}{\sigma_i^2}\left(\frac{\mathbf{T}\mathbf{T}^T}{\sigma_i^2}\right)^{-1}. \tag{2-35}$$

To incorporate the data standard deviations (σ_i) in the solution, the system of equations is scaled to obtain a weighted system of equations. Therefore we define matrix $\mathbf{W}$ as diag($1/\sigma_1$, $1/\sigma_2$,.....,$1/\sigma_m$) and set

$$\mathbf{W}\,\mathbf{r}=\mathbf{r}_w$$
$$\mathbf{W}\,\mathbf{T}=\mathbf{T}_w.$$

The MLE of $\mathbf{p}$ is then

$$\hat{\mathbf{p}}_{\mathrm{MLE}}=\mathbf{r}_w\mathbf{T}_w^T\left(\mathbf{T}_w\mathbf{T}_w^T\right)^{-1}. \tag{2-36}$$

This MLE estimator is implemented in Matlab and the impulse response is estimated. These results are discussed in the next chapter.

2-3-2 Blind deconvolution

The output DTS data ($\mathbf{r}$) is only known, so with the blind deconvolution method both the input data $\mathbf{t}$ and impulse response ($\mathbf{p}$) are estimated. For this estimation the Matlab function "deconvblind.m" is used. The function "deconvblind.m" uses as input the DTS output data and an initial impulse response. The initial impulse response is defined as a vector of ones.

The Matlab "deconvblind.m" algorithm works as follows:

Again Eq. (2-26) is assumed. Now we solve for $\mathbf{r}=\mathbf{P}\mathbf{t}$, because the noise is already included in the available DTS data $\mathbf{r}$. Subsequently the input temperature $\mathbf{t}$ is determined as

$$\hat{\mathbf{t}}=\mathbf{r}\mathbf{P}^T\left(\mathbf{P}\mathbf{P}^T\right)^{-1}. \tag{2-37}$$

Directly evaluating this expression will lead to a bad estimate of the input due to amplification of noise. The error between the real and estimated input need to be minimized. This problem is a regularization problem and the following equation needs to be minimized [5]

$$\hat{\mathbf{T}}(\omega)=\mathrm{argmin}\Big[\lambda||\mathbf{R}(\omega)-\hat{\mathbf{P}}(\omega)\hat{\mathbf{T}}(\omega)||^2+||\mathbf{Q}(\omega)\hat{\mathbf{T}}(\omega)||^2\Big]. \tag{2-38}$$

Eq. (2-38) is solved in the Fourier domain, therefore $\mathbf{r}$, $\mathbf{t}$ and $\mathbf{P}$ are Fourier transformed (FFT) to respectively $\mathbf{R}(\omega)$, $\mathbf{T}(\omega)$ and $\mathbf{P}(\omega)$ and $\mathbf{Q}(\omega)$ is chosen as $\mathbf{T}(\omega)^{-1}$. Finally, λ is the regularization parameter.

In order to minimize Eq. (2-38), the gradient of $\hat{\mathbf{T}}(\omega)$ is set to zero and this equation becomes

$$-2\lambda\hat{\mathbf{P}}(\omega)\mathbf{R}(\omega)+2\lambda\hat{\mathbf{P}}^{*}(\omega)\hat{\mathbf{P}}(\omega)\hat{\mathbf{T}}(\omega)+2\mathbf{Q}^{*}(\omega)\mathbf{Q}(\omega)\hat{\mathbf{T}}(\omega)=0. \tag{2-39}$$

Solving Eq. (2-39) for $\hat{\mathbf{T}}(\omega)$ leads to

$$\hat{\mathbf{T}}(\omega)=\lambda\hat{\mathbf{P}}^{*}(\omega)\mathbf{R}(\omega)\Big(\lambda|\hat{\mathbf{P}}(\omega)|^{2}+|\hat{\mathbf{Q}}(\omega)|^{2}\Big)^{-1}. \tag{2-40}$$

Now the impulse response needs to be estimated. By solving Eq. (2-36) in the previous section, it was shown that this leads to a bad estimation of the impulse response due to high amplification of the noise. Similar to the estimation of the input, the impulse response estimation is also a regularization problem. The following equation needs to be minimized [5]

$$\hat{\mathbf{P}}(\omega)=\operatorname{argmin}\Big[\lambda||\mathbf{R}(\omega)-\hat{\mathbf{P}}(\omega)\hat{\mathbf{T}}(\omega)||^{2}+||\mathbf{Q}(\omega)\hat{\mathbf{P}}(\omega)||^{2}\Big]. \tag{2-41}$$

Eq. (2-41) is solved in the Fourier domain, therefore $\mathbf{r}$, $\mathbf{t}$ and $\mathbf{P}$ are Fourier transformed (FFT) to respectively $\mathbf{R}(\omega)$, $\mathbf{T}(\omega)$ and $\mathbf{P}(\omega)$ and $\mathbf{Q}(\omega)$ is chosen as $\mathbf{P}(\omega)^{-1}$. Finally, λ is the regularization parameter.

In order to minimize Eq. (2-41), the gradient of $\hat{\mathbf{P}}(\omega)$ is set to zero and Eq. (2-41) becomes

$$-2\lambda\hat{\mathbf{T}}(\omega)\mathbf{R}(\omega)+2\lambda\hat{\mathbf{T}}^{*}(\omega)\hat{\mathbf{T}}(\omega)\hat{\mathbf{P}}(\omega)+2\mathbf{Q}^{*}(\omega)\mathbf{Q}(\omega)\hat{\mathbf{P}}(\omega)=0. \tag{2-42}$$

Solving Eq. (2-42) for $\hat{\mathbf{P}}(\omega)$ leads to

$$\hat{\mathbf{P}}(\omega)=\lambda\hat{\mathbf{T}}^{*}(\omega)\mathbf{R}(\omega)\Big(\lambda|\hat{\mathbf{T}}(\omega)|^{2}+|\hat{\mathbf{Q}}(\omega)|^{2}\Big)^{-1}. \tag{2-43}$$

The initial impulse response is defined as a vector of ones (as mentioned before). With this initial impulse response the first input $\hat{\mathbf{T}}(\omega)$ is estimated by using Eq. (2-40). After having estimated the input $\hat{\mathbf{T}}(\omega)$, this new estimate of $\hat{\mathbf{T}}(\omega)$ is plugged into Eq. (2-43) and the impulse response $\hat{\mathbf{P}}(\omega)$ is estimated. These steps are repeated until there is a good reconstruction of the output data.

Chapter 3

Results

In this chapter we illustrate the performance of the two deconvolution methods. In the first section of this chapter, the results of the impulse response estimate are discussed. The impulse response is estimated with the MLE method and the blind deconvolution method. It is shown that the MLE method performs better than the blind deconvolution method. In the second section the results of the input temperature are discussed. It is demonstrated that the total variation deconvolution method gives better input temperature results than the blind deconvolution method. Finally, in the third section the spatial resolution increase is discussed. The spatial resolution is executed by interpolation in the Fourier domain.

3-1 Results Impulse Response

The impulse response is estimated first by assuming an ideal input and implementing the MLE estimator from Eq. (2-36) in Matlab. The second method which is used to estimate the impulse response is by implementing the blind deconvolution algorithm, as discussed in chapter 2-3-2, in Matlab.

3-1-1 Ideal Input

The ideal input temperature is assumed over the full fiber optic cable length of 90m. The estimated impulse response is shown in Figure 3-1. The impulse response is also estimated with the "impulseest.m" function of Matlab. This function also uses the MLE method as discussed in section 2-3-1, but it also implements regularization. The regularization suppresses noise, especially for bad pixels this is very important and hence it gives a slightly better estimate of the impulse response (see Figure 3-2).

It is observed that both impulse responses are similar, the small difference is due to the regularization which Matlab uses.

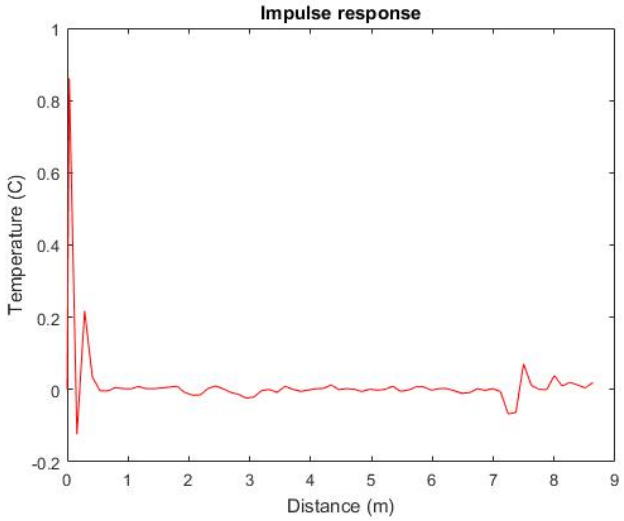

Figure 3-1: impulse response estimated with MLE

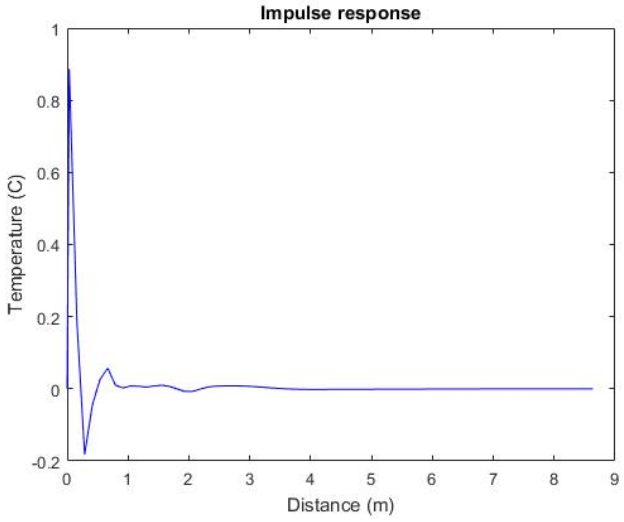

Figure 3-2: impulse response estimated with Matlab algorithm

In order to verify if the impulse response is estimated accurately, the DTS output data is reconstructed. The output data is shown in Figure 3-3 and it is observed that the data reconstruction is not good enough.

The output data is also reconstructed with the impulse response which is estimated with the "impulseest.m" function from Matlab. The output data is shown in Figure 3-4 and also in this case the reconstructed data is not good enough. Therefore the impulse response plotted in Figure 3-1 and the impulse response plotted in Figure 3-2 cannot be accepted. This does not mean that the MLE method is not good to estimate the impulse response. It means that the assumption of an ideal input over the full fiber optic cable length gives a bad estimate of the impulse response and a bad output data reconstruction.

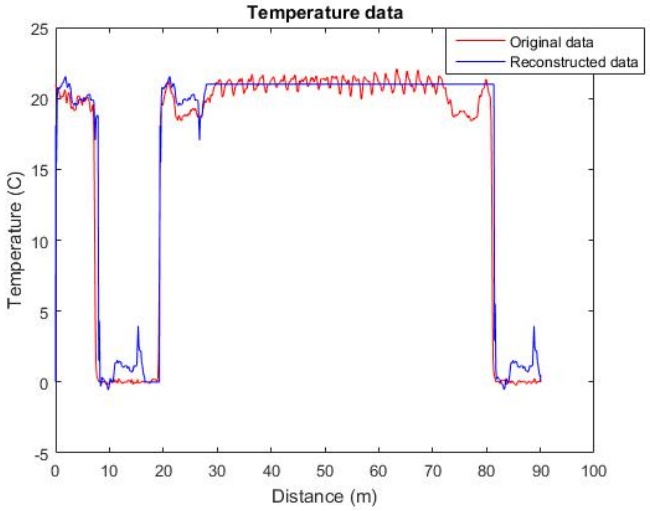

Figure 3-3: data estimated with MLE method

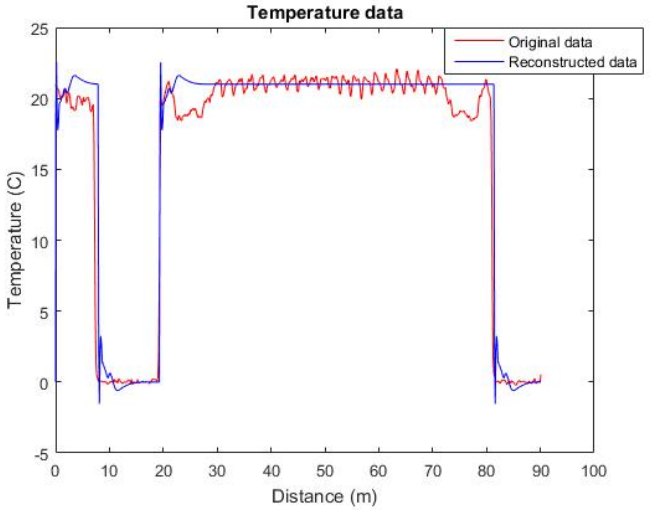

Figure 3-4: data estimated with impulseest function Matlab

It is not correct to assume ideal input over the full cable length of 90m, because the input temperature is not known between 20m and 80m and by assuming ideal input between 20m and 80m important information about the temperature is lost. The input temperature is only known between 10m-20m and after 80m, because at these distances the cable is put into an ice bath, hence the input temperature is around 0°C. The impulse response will now be estimated with the temperature output data between 10m-20m,because at this distance the input temperature is known and thus it will result in a more reliable estimate of the impulse response. The impulse response is again estimated with the MLE estimator from Eq. (2-36) and shown in Figure 3-5. This impulse response is different than the impulse responses shown in Figure 3-1 and Figure 3-2 but in section 3-1-2 it is shown that this impulse response is also obtained with the blind deconvolution algorithm.

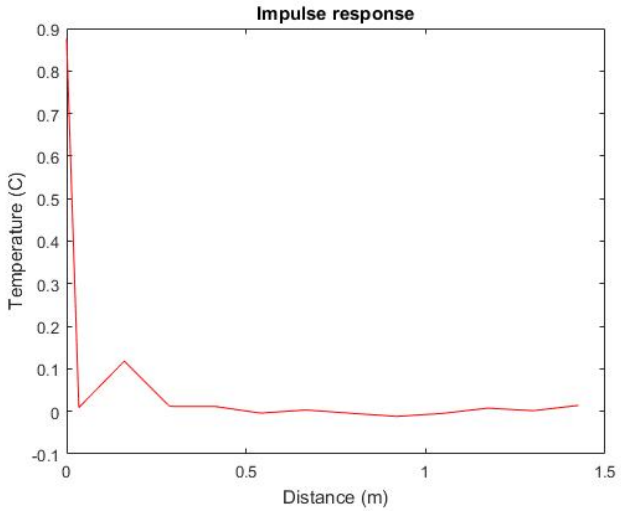

Figure 3-5: Impulse response DTS

3-1-2 Blind Deconvolution

The only data which is available is the DTS output data (both the impulse response and input data are not known). Therefore the blind deconvolution method is used in order to estimate the impulse response.

The impulse response is estimated by using the "deconvblind.m" function of Matlab. This impulse response is shown in Figure 3-6. The initial guess of the impulse response is a vector of ones.

From Figure 3-6 it is observed that the estimated impulse response is not similar to the estimated impulse response shown in Figure 3-5. The amplitude is also not similar to the amplitude of the impulse response shown in Figure 3-5. This occurs due to the fact that Matlab normalizes the impulse response which means that the sum of all samples of the impulse response is summed to one. The impulse response in Figure 3-6 consists of 700 samples whereas the impulse response in Figure 3-5 consists of 13 samples. The impulse response in Figure 3-5 is limited to only 13 samples because the input data is limited and consists of only 128 samples. The impulse response after 13 samples goes to zero. From

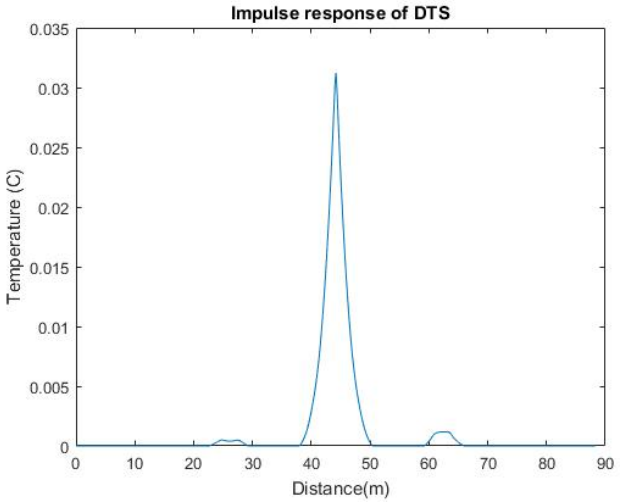

Figure 3-6: Impulse response estimated with blind deconvolution

Figure 3-6 the nature of the estimated impulse response is not clear. After curve fitting in Matlab it is shown that this impulse response is an exponential impulse response. The curve fitting is shown in Figure 3-7. The estimated impulse response is shown in blue, the exponential impulse response is shown in red and the Gaussian impulse response is shown in black. The function of the exponential impulse response is: $0.0024^{0.1x-30} + 1.47^{-0.1x-30}$.

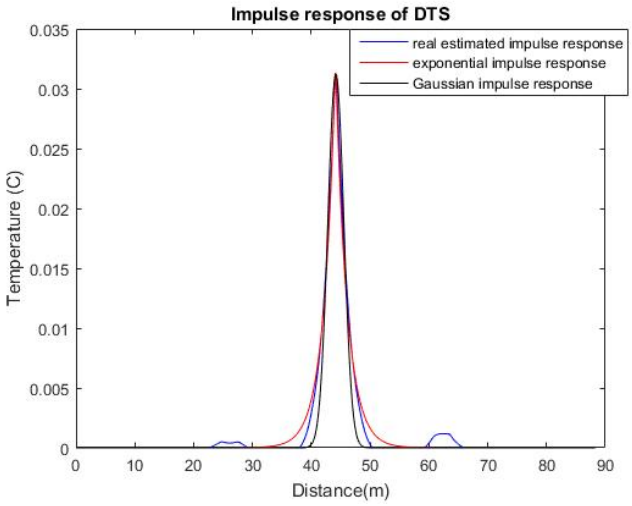

Figure 3-7: Curve fitting blind deconvolution

The function of the Gaussian impulse response is: $0.03122e^{[-((x-351)^2)/230]}$. From the curve fitting it is still not clear what the nature of the impulse response is, because all the impulse responses are really close. Therefore the RMS errors are calculated to draw a conclusion. The RMS error between the exponential-and estimated impulse response is equal to $5.25 * 10^{-4}$. The RMS error between the Gaussian-and estimated impulse response is equal to $9.7 * 10^{-4}$ which is larger than the previous RMS error. Based on this error criterion, we conclude that an exponential impulse response provides a better fit.

Now it is investigated if the estimated impulse response gives the correct DTS output temperature by convolving the DTS impulse response with the obtained (from the blind deconvolution) input temperature. This is shown in Figure 3-8. Figure 3-8 shows that the reconstructed output data (in blue) is more blurry compared to the measured original output data (in red). The temperature decrease from hot object to ice bath is also less sharp than the temperature decrease of the original measured output data. The temperature between 20m and 80m is also not estimated well. Reason for this blurry reconstruction is that the impulse response estimated with the blind deconvolution algorithm is not good. The blind deconvolution algorithm strongly depends on the initial guess of the impulse response. If there is a bad initial guess of the impulse response then it also will give a bad impulse response estimate.

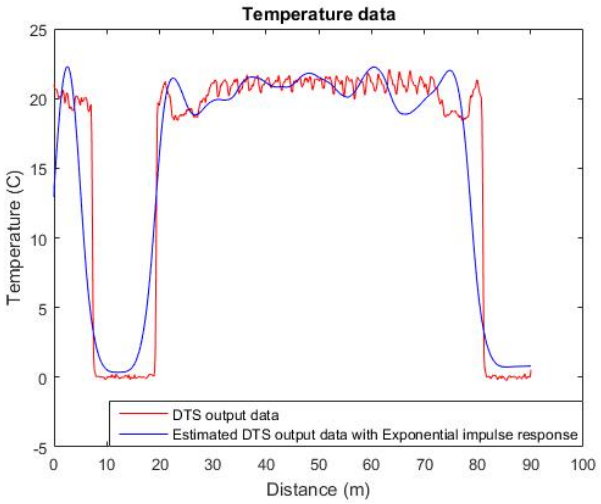

Figure 3-8: Output data estimated with blind deconvolution

The blind deconvolution algorithm is retried with a new initial guess of the impulse response. This new initial guess of the impulse response, is the impulse response shown in Figure 3-5 which was obtained with the MLE method. The new impulse response estimate is shown in Figure 3-9. This impulse response is very similar to the impulse response shown in Figure 3-5.

The DTS output data is reconstructed by convolving the new DTS impulse response estimate with the DTS input temperature (obtained from blind deconvolution). This is shown in Figure 3-10. It is clearly observed that the reconstruction of the output data is much better now, except for the sharp edge at 80m. This occurs due to the finite Fourier transformation and it is further explained in the next chapter.

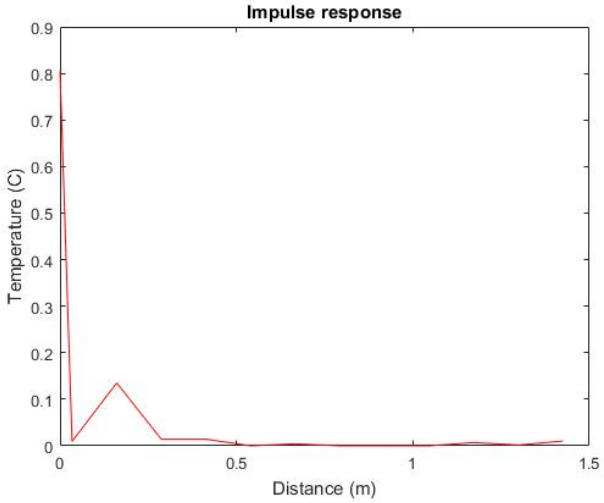

Figure 3-9: New impulse response estimated with blind deconvolution

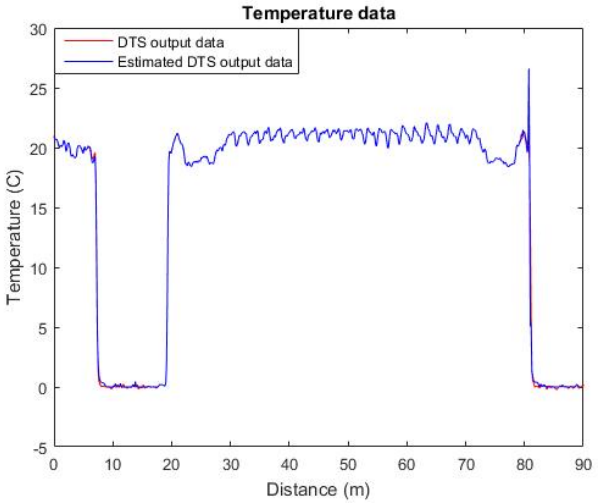

Figure 3-10: New output data estimated with blind deconvolution

3-2 Results for Real Input Temperature of DTS

In this section the DTS input temperature is estimated by using three methods, namely assuming ideal input over a part of the fiber optic cable, blind deconvolution and assuming a Gaussian impulse response.

3-2-1 Ideal Input

In section 3-1-1 it has been shown that assuming ideal input temperature over the whole fiber optic cable length is not correct. Ideal input temperature can only be assumed between 10m-20m because at this distance the input temperature is known as the fiber is in an ice bath of approximately 0°C. In this section the input temperature is reconstructed by deconvolving the full DTS output temperature with the impulse response shown in Figure 3-5 (when input temperature is assumed ideal only between 10m-20m). To obtain the input temperature, the total variation deconvolution algorithm is used which is described in section 2.2. The DTS input and output temperatures are illustrated in Figure 3-11.

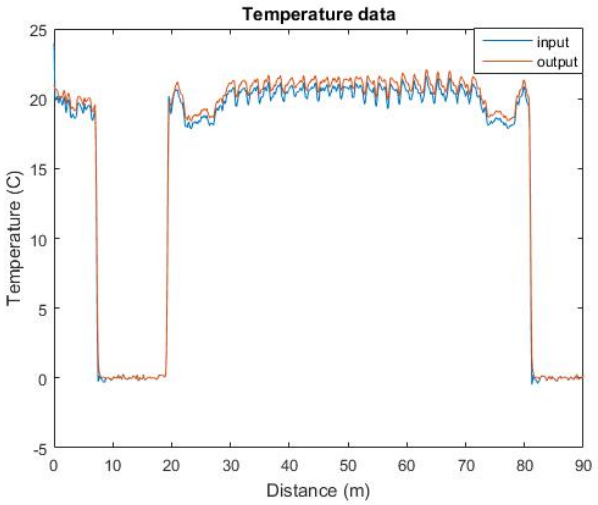

Figure 3-11: DTS input temperature

The input temperature is on average approximately 0.43°C smaller than the output temperature. This is correct because the output temperature is measured by the DTS with measurement errors. With the total variation deconvolution algorithm these measurement errors are minimized and the input temperature is correctly estimated. It is good to know the input temperature because now there is a better (less blurry) and more reliable estimate of the patient's temperature inside the 7T MRI scanner.

To check whether the temperature decrease/increase from a hot object to the ice bath and vice-versa is more steep, Figure 3-11 is zoomed in and shown in Figure 3-12.

From Figure 3-12 it is observed that the input temperature decrease/increase is indeed more steep than the output temperature increase/decrease. This is reasonable because measurement errors due to noise are minimized.

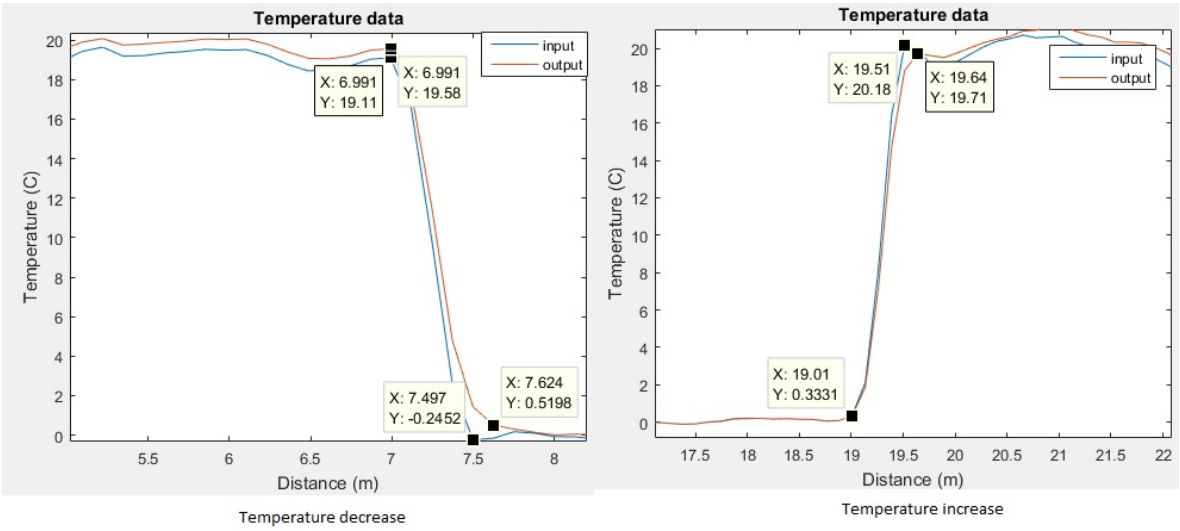

Figure 3-12: DTS machine resolution

The distance which is needed for the temperature to decrease/increase from a hot object to the ice bath is called the machine resolution. The machine resolution for the input temperature is 51cm and the machine resolution of the output temperature is 63cm. There is a machine resolution improvement of 12cm (19%) when the input temperature of the DTS is estimated with the total variation deconvolution algorithm. This is beneficial when the geometry of the fiber optic cable is changed from a 2D raster to a 3D coil. The coil resolution is given as [12]

$$\text{coil resolution} = \frac{\text{machine resolution}}{L}. \tag{3-1}$$

The coil resolution is the effective spatial resolution of the temperature measurement. In Eq. (3-1), L is equal to the diameter of the coil. To measure the temperature with a coil resolution of at least 5cm, the coil diameter should be 10cm as the machine resolution is 51cm. If there is a better machine resolution there will also be a better coil resolution, which means that the temperature can be estimated with a better spatial resolution if a 3D coil geometry is used.

3-2-2 Blind Deconvolution

In this subsection the input temperature of the DTS is estimated with the blind deconvolution algorithm as discussed in the previous chapter. First the initial guess of the impulse response was a vector of ones and it was found that this guess was not correct. Figure 3-13 shows the DTS input temperature which is found with the first initial guess of the impulse response.

From Figure 3-13 it is observed that there is an overshoot at the edges, called Gibbs effect. Also the machine resolution became worse after the blind deconvolution algorithm. The Gibbs effect occurs because the blind deconvolution algorithm works in the Fourier domain as explained in the previous chapter on a finite data set. It is difficult to approximate a discontinuous function by a finite series of continuous cosine and sine waves. The n^{th}

partial sum of the Fourier series has large oscillations near the jump which might increase the maximum of the partial sum above the function itself. As n increases the overshoot does not die out but approaches a finite limit [11].

The DTS input temperature shown in Figure 3-13 is not correctly estimated with the initial guess of the impulse response. Therefore the input temperature is estimated by using the impulse response, obtained from the ideal input method, as an initial guess for the blind deconvolution algorithm. This is shown in Figure 3-14.

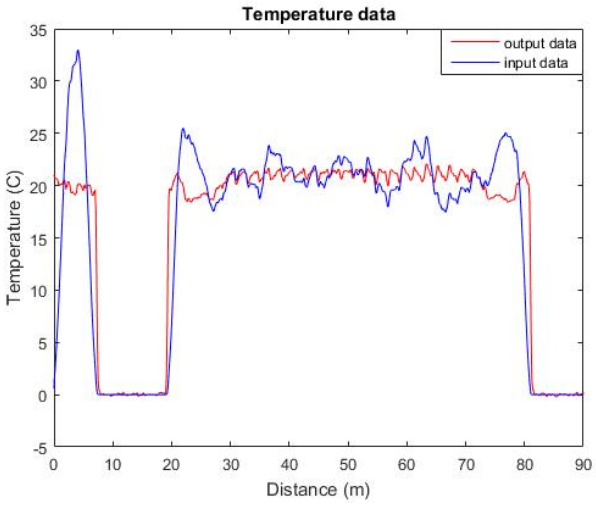

Figure 3-13: DTS input temperature blind deconvolution

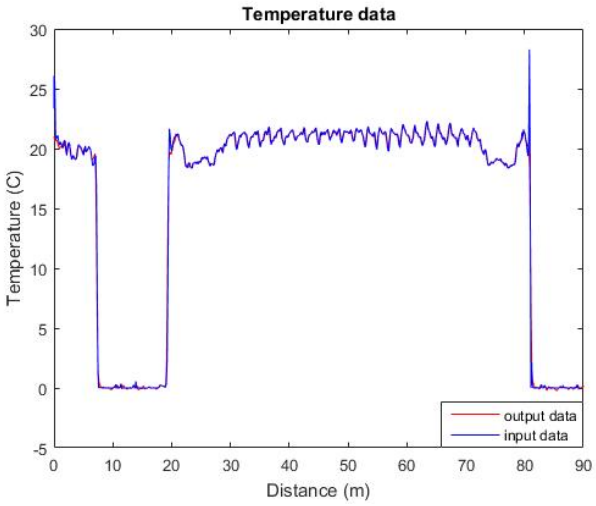

Figure 3-14: DTS input temperature blind deconvolution with new impulse response

Figure 3-14 illustrates that the input data still has a sharp overshoot at the edges but it is better than the previous impulse response shown in Figure 3-13. The input temperature is approximately equal to the output temperature, which is not good. The blind deconvolution algorithm does not give an accurate estimate of the input temperature. The measurement errors are not minimized good enough. The machine resolution improvement is also investigated.

Figure 3-15 shows the temperature decrease/increase from a hot object to an ice bath and vice-versa. From this figure the machine resolution is obtained. The machine resolution for the DTS output temperature is 63cm as shown in Figure 3-15 and the machine resolution of the DTS input temperature is 51cm. This is the same machine resolution improvement of 19%, which was obtained with the ideal input method. Hence the blind deconvolution algorithm does not improve the DTS temperature estimation but it does improve the machine resolution of the DTS.

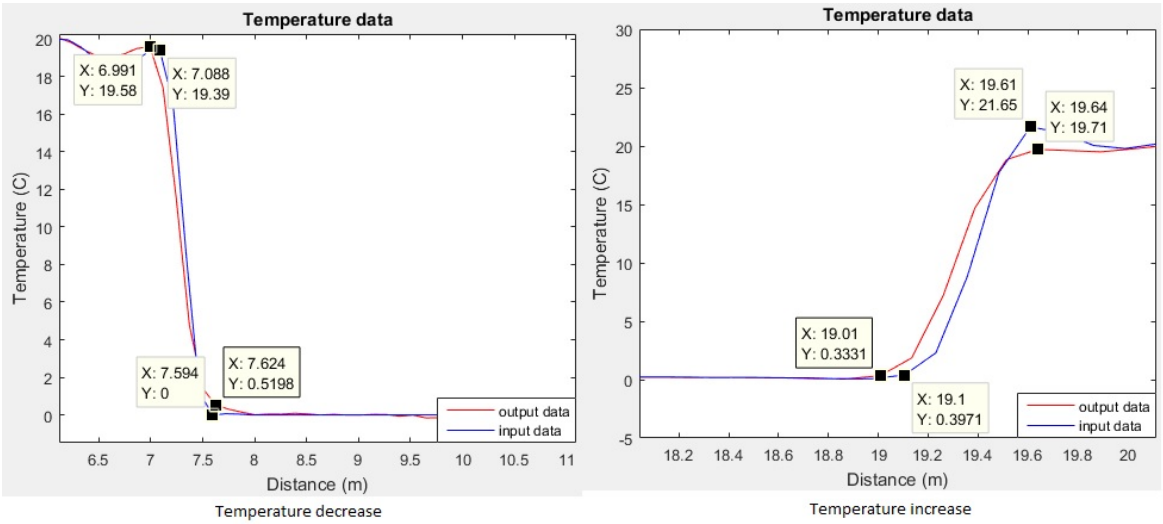

Figure 3-15: DTS machine resolution blind deconvolution with new impulse response

3-2-3 Gaussian Impulse Response

In this subsection the impulse response ($\mathbf{p}$) is assumed Gaussian. This Gaussian impulse response is deconvolved with the DTS output data by using the total variation deconvolution algorithm discussed in section 2-2, in order to obtain the real input temperature. The obtained input temperature is shown in Figure 3-16.

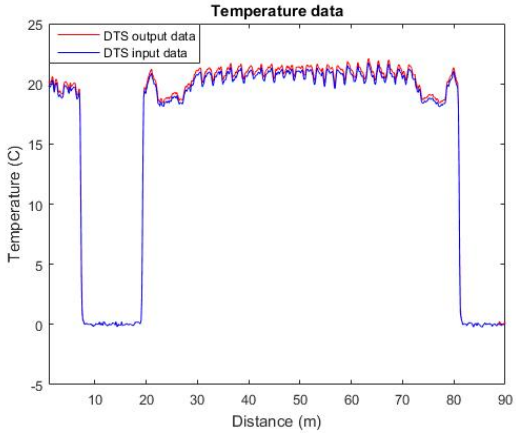

Figure 3-16: DTS input temperature with Gaussian impulse response

From Figure 3-16 it is observed that the DTS input temperature estimate is not bad. The input temperature is on average 0.27°C less than the output temperature. For the ideal input method the input temperature was 0.43°C less than the output temperature. This difference is due to the fact that a Gaussian impulse response is assumed but from the ideal input method an exponential impulse response was obtained, which is better than the Gaussian impulse response if we look at the curve fitting from section 3-1-2.

The machine resolution improvement is also investigated. Figure 3-17 illustrates the temperature decrease/increase from a hot object to an ice bath and vice-versa. From this figure the machine resolution is obtained. The machine resolution for the DTS output temperature is 63cm as shown in Figure 3-17 and the machine resolution of the DTS input temperature is 51cm. This is the same machine resolution improvement of 19%. which was obtained with the ideal input method. Hence assuming a Gaussian impulse response and deconvolving the DTS output with the Gaussian impulse response, using the total variation deconvolution method, does improve the machine resolution of the DTS.

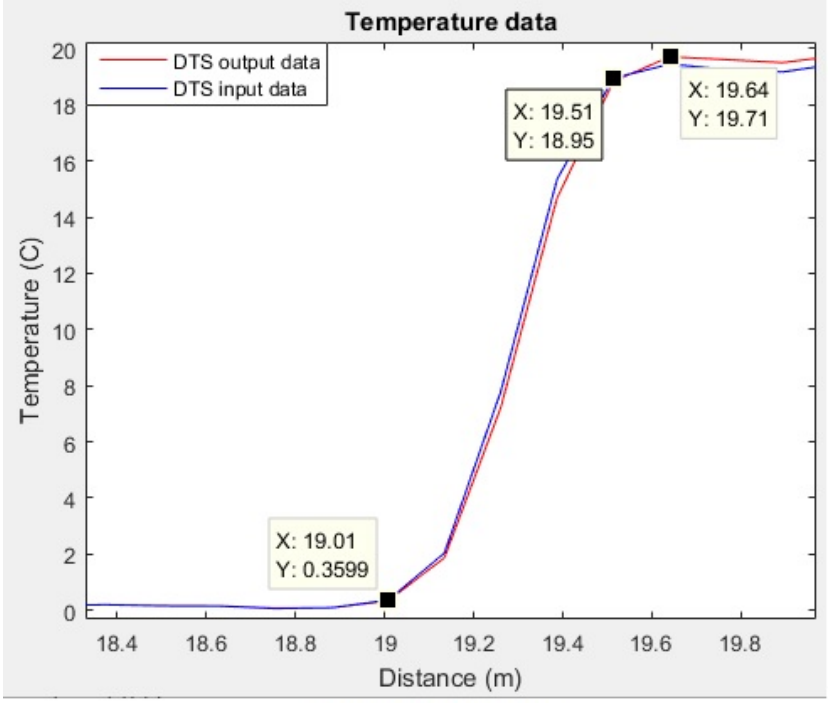

Figure 3-17: DTS machine resolution with Gaussian impulse response

3-3 Results for Spatial Resolution Increase of DTS

In this section the spatial resolution of the fiber optic temperature sensor will be increased by Fourier domain interpolation. In this way the temperature estimate for more measured points will still be accurate. The interpolation in Fourier domain is performed by transforming the input temperature to the Fourier domain (FFT) and pad it with zeros between the positive and negative part of the Fourier signal.

The more zeros are padded the more points of the temperature estimate are obtained. After the interpolation the signal is transformed back to the time domain (IFFT). The spatial resolution increase will be performed on the DTS input temperature which is obtained by three methods, namely: Ideal input, Blind deconvolution and Gaussian impulse response.

3-3-1 Ideal Input

In this section the results of the spatial resolution increase is discussed when ideal input temperature is assumed between 10m-20m. This is shown in Figure 3-18. The input temperature is 0.43°C below the output temperature. Reasons for this is mentioned in the previous section. The temperature is estimated on every 6.3cm instead of 12.6cm. The spatial resolution was increased by a factor of two. However, by increasing the spatial resolution by a factor of two, the machine resolution decreases and this is shown Figure 3-19.

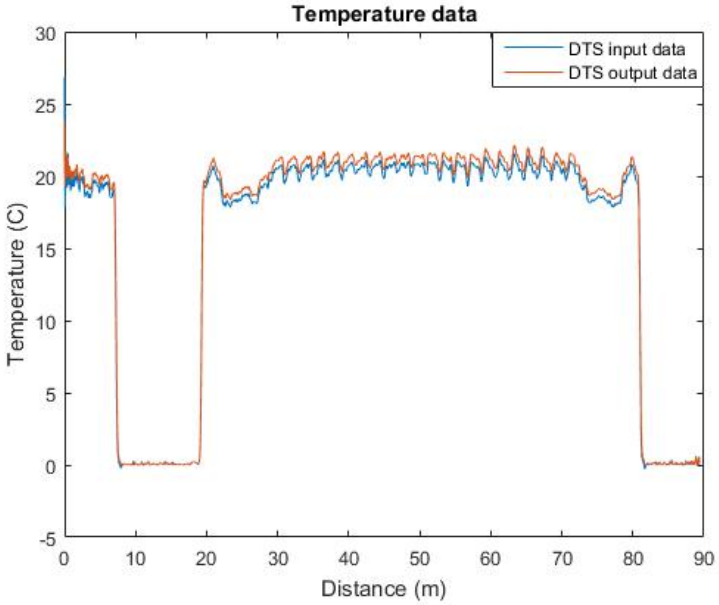

Figure 3-18: DTS input temperature with resolution of 6.3cm

From Figure 3-19 it is observed that the machine resolution is 70cm. Earlier it was mentioned that the machine resolution improved to 51cm, but after increasing the spatial resolution it decreased to 70cm. This is a decrease of 37%. This decrease is expected because the temperature is estimated on more points and due to the interpolation between points the temperature decrease/increase will be less steep. The more the spatial resolution is increased, the more the machine resolution is decreased.

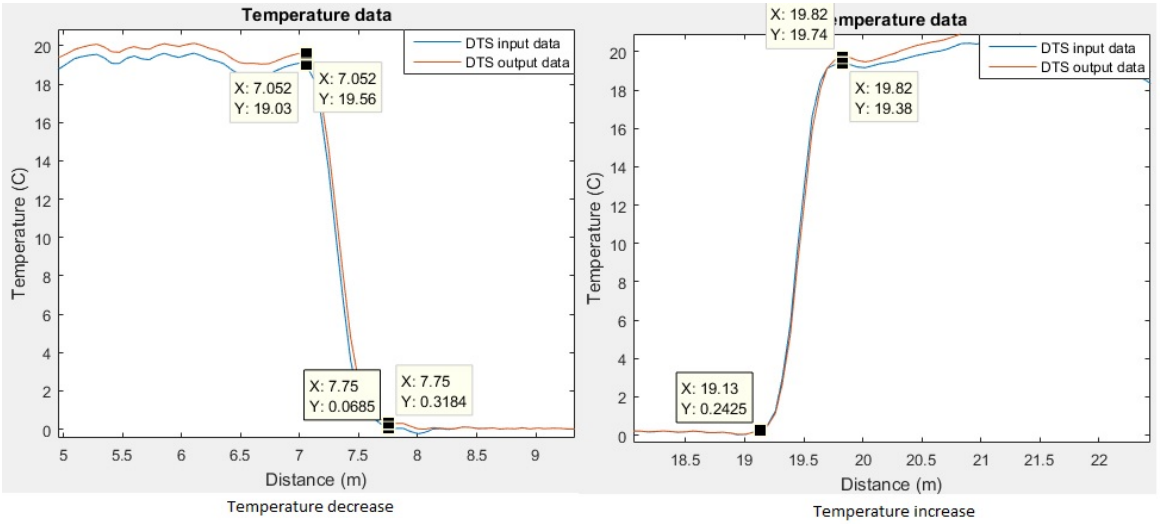

Figure 3-19: DTS machine resolution with spatial resolution of 6.3cm

For the second case, the spatial resolution is increased by a factor of four and the resulting machine resolution is shown in Figure 3-20. The temperature estimate is for every 3.15cm. The machine resolution in this case is 78cm. This machine resolution compared to the previous achieved machine resolution of 51cm, is 27cm (53%) larger.

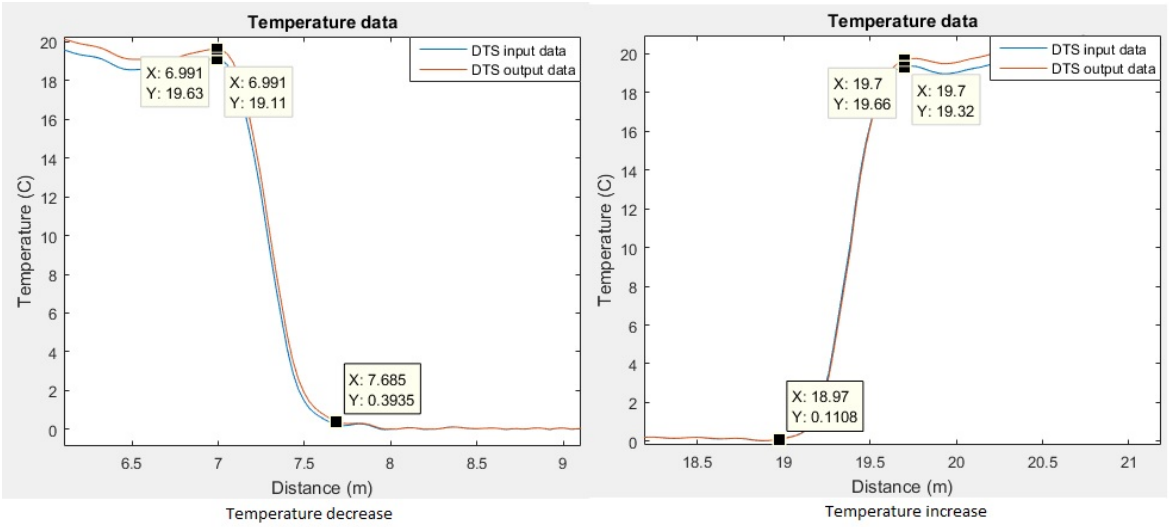

Figure 3-20: DTS machine resolution with spatial resolution of 3.15cm

The spatial resolution is finally increased by a factor of eight and the resulting machine resolution is shown in Figure 3-21. In this case the temperature estimate is obtained for every 1.58cm. The machine resolution in this case is 80cm. So compared to the machine resolution of 51cm this is a decrease of 31cm (58%).

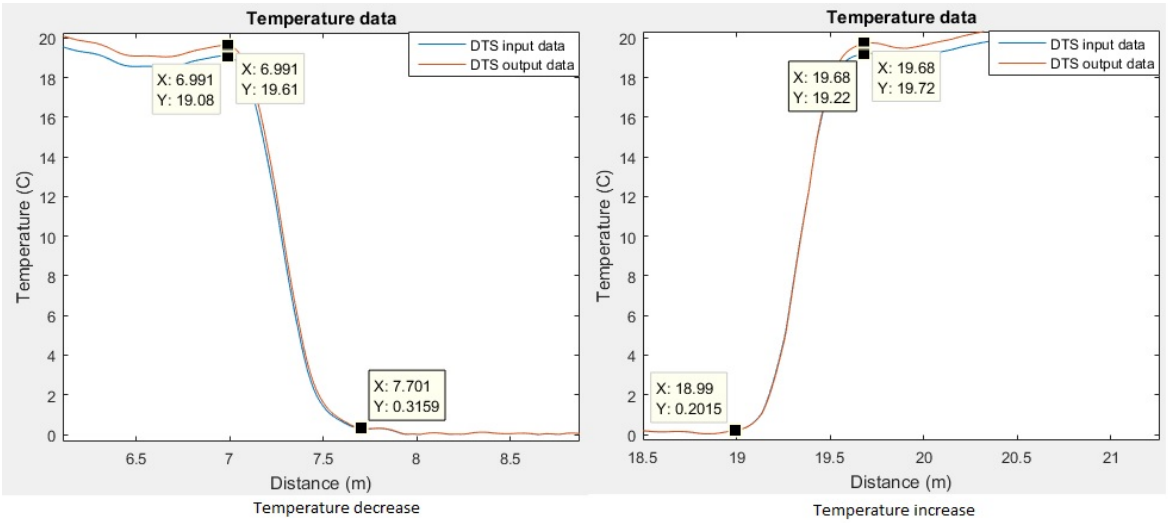

Figure 3-21: DTS machine resolution with spatial resolution of 1.58cm

Spatial-resolution (cm)	**Machine-resolution (cm)**	**Machine-resolution decrease (cm)**	**Machine-resolution decrease**
12.5	51	NA	NA
6.3	70	19	37%
3.15	78	27	53%
1.58	80	31	58%

Table 3-1: Summary resolution ideal input

The spatial- and machine resolution results are summarized in Table 3-1. To validate the total variation deconvolution algorithm, the input temperature is estimated for another temperature measurement. This is shown in Figure 3-22.

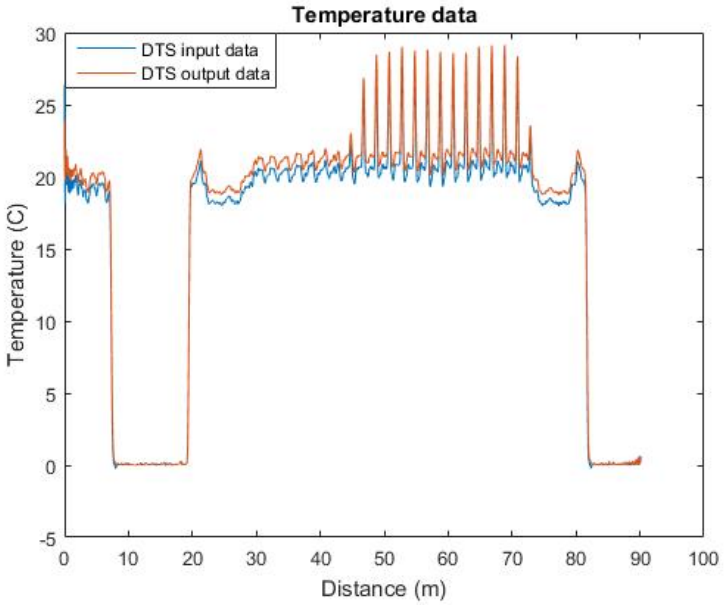

Figure 3-22: DTS input temperature with resolution of 6.3cm for second measurement

From Figure 3-22 it is observed that the DTS input data is below the DTS output data. There is a difference of 0.43°C, which is the same as for the previous measurement. Also the spikes between 50m and 80m are perfectly reconstructed. This means that the total variation deconvolution algorithm and the impulse response, which are used to estimate the input temperature, are correct. In Figure 3-23 the machine resolution is shown. The machine resolution is 70cm, which is the same as the previous measurement when the spatial resolution is increased by a factor of two. When the spatial resolution is increased by a factor of four and a factor of eight, the machine resolution remains the same as in the previous measurement, respectively 78cm and 80cm.

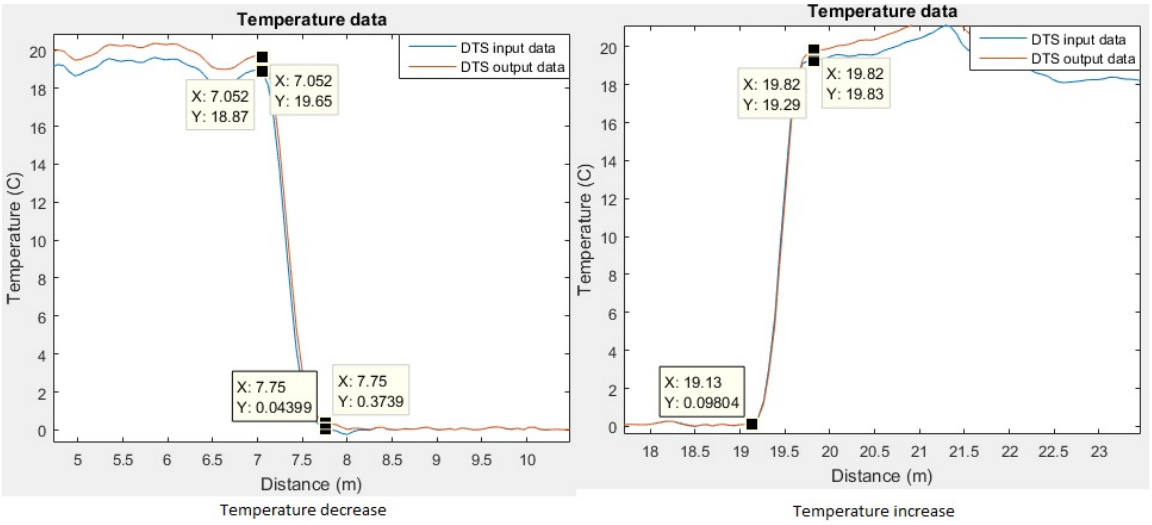

Figure 3-23: DTS machine resolution for second measurement

3-3-2 Blind Deconvolution

In this section the results of the spatial resolution increase is discussed when the input temperature is obtained with the blind deconvolution method. This is shown in Figure 3-24. The input temperature is similar to the output temperature. Reasons for this are mentioned in section 3-2-2. The temperature estimate is first obtained for every 6.3cm instead of 12.6cm. This is a spatial resolution increase by a factor of two. However, increasing the spatial resolution by a factor of two, the machine resolution decreases, as shown in Figure 3-25.

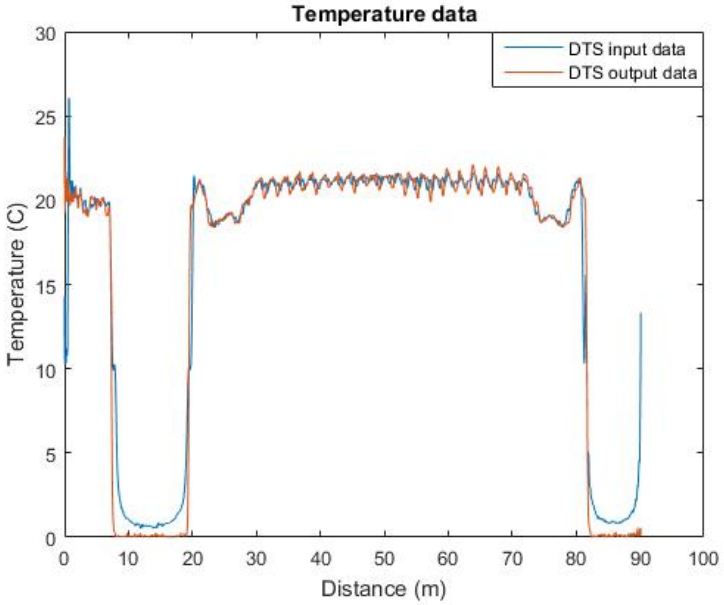

Figure 3-24: DTS input temperature with resolution of 6.3cm for blind deconvolution

From Figure 3-25 it is observed that the machine resolution increases to 230cm, after blind deconvolution. Earlier it was mentioned that the machine resolution improved to 51cm, but after increasing the spatial resolution it decreased to 230cm. This is a decrease of 451%. This decrease is expected because the temperature is estimated on more points and due to the interpolation between points the temperature decrease/increase will be less steep. The more the spatial resolution is increased, the more the machine resolution is decreased.

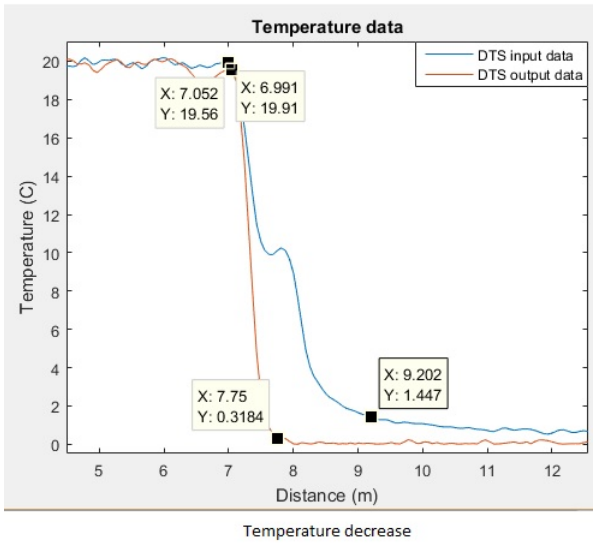

Figure 3-25: DTS machine resolution for blind deconvolution and spatial resolution of 6.3cm

We increase the spatial resolution by a factor of four and the resulting machine resolution is shown in Figure 3-26. The temperature estimate is for every 3.15cm. In this case the machine resolution is 240cm. This is a decrease of 189cm (471%) when compared to the machine resolution of 51cm .

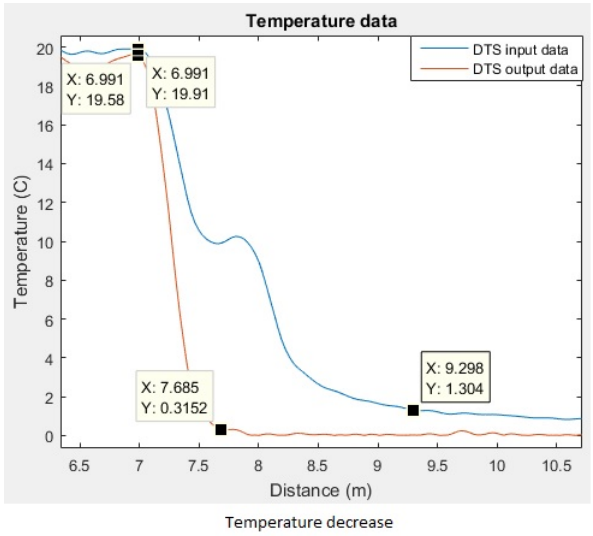

Figure 3-26: DTS machine resolution for blind deconvolution and spatial resolution of 3.15cm

Finally, the spatial resolution is increased by a factor of eight and the resulting machine resolution is shown in Figure 3-27. The temperature estimate is obtained for every 1.58cm The machine resolution is in this case 246cm. So compared to the machine resolution of 51cm this is a decrease of 195cm (482%).

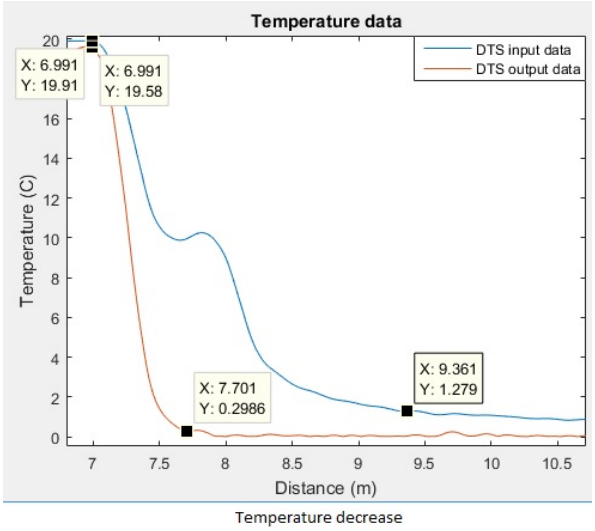

Figure 3-27: DTS machine resolution for blind deconvolution and spatial resolution of 1.58cm

Spatial-resolution (cm)	**Machine-resolution (cm)**	**Machine-resolution decrease (cm)**	**Machine-resolution decrease**
12.5	51	NA	NA
6.3	230	179	451%
3.15	240	189	471%
1.58	246	195	482%

Table 3-2: Summary resolution blind deconvolution

The spatial- and machine resolution results are summarized in Table 3-2. To validate the blind deconvolution algorithm, the input temperature is estimated for another temperature measurement as shown in Figure 3-28.

From Figure 3-28 it is observed that the spikes between 50m and 80m between the input temperature and output temperature shows a large difference. This difference is approximately 3°C. From this validation, it is concluded that the blind deconvolution algorithm does not accurately estimate the input temperature. Reason for this is that the blind deconvolution algorithm strongly depends on the initial guess of the impulse response. If the initial guess is bad, the estimated input data will also be wrong. In Figure 3-29 the machine resolution is shown. The machine resolution when using blind deconvolution is 230cm, which is the same as the previous measurement when the spatial resolution is increased by a factor of two. When the spatial resolution is increased by a factor of four and by a factor of eight, the machine resolution remains the same as in the previous measurement, respectively 240cm and 246cm.

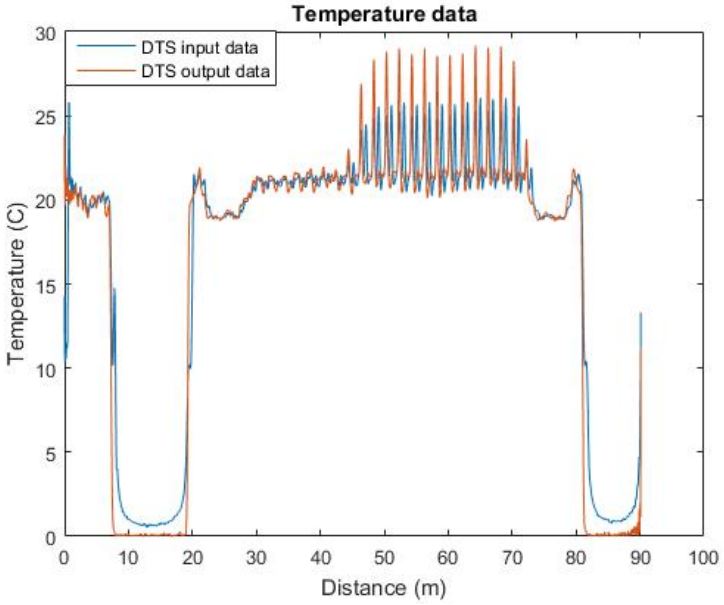

Figure 3-28: Input temperature resolution of 6.3cm second measurement blind deconvolution

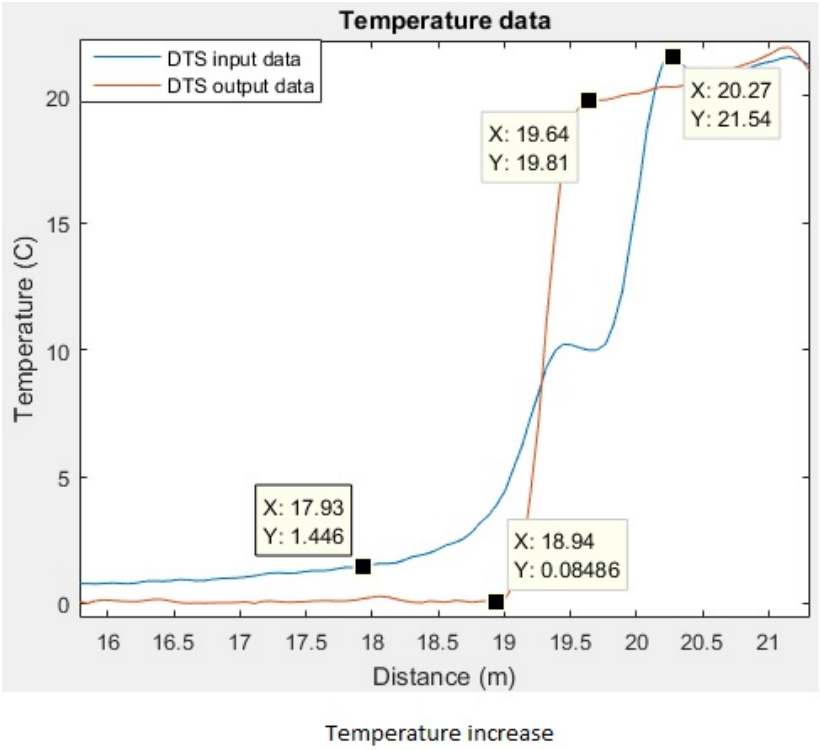

Figure 3-29: DTS machine resolution for second measurement blind deconvolution

3-3-3 Gaussian Impulse Response

In this section the results of the spatial resolution increase are discussed when a Gaussian impulse response is assumed. This is shown in Figure 3-30. The input temperature is 0.27°C below the output temperature. Reasons for this are mentioned in the previous section. The temperature is estimated for every 6.3cm instead of 12.6cm. This is a spatial resolution increase by a factor of two. However, increasing the spatial resolution by a factor of two, the machine resolution decreases, this is shown Figure 3-31.

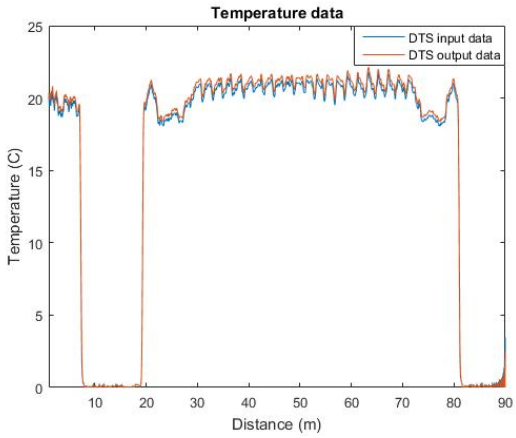

Figure 3-30: DTS input temperature with resolution of 6.3cm for Gaussian impulse response

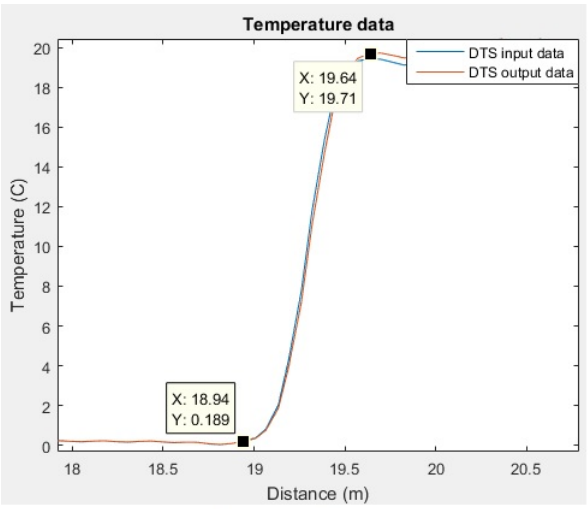

Temperature increase

Figure 3-31: Machine resolution for Gaussian impulse response and spatial resolution of 6.3cm

From Figure 3-31 it is observed that the machine resolution is 70cm. Previous it was mentioned that the machine resolution improved to 51cm, but after increasing the spatial resolution it decreased to 70cm. This is a decrease of 37%. This decrease is expected because the temperature is estimated on more points and due to the interpolation between points the temperature decrease/increase will be less steep. The more the spatial resolution is increased, the more the machine resolution is decreased.

The spatial resolution is increased by a factor of four and the resulting machine resolution is shown in Figure 3-32. The temperature estimate obtained for every 3.15cm. The machine resolution is 78cm. So compared to the machine resolution of 51cm this is a decrease of 27cm (53%).

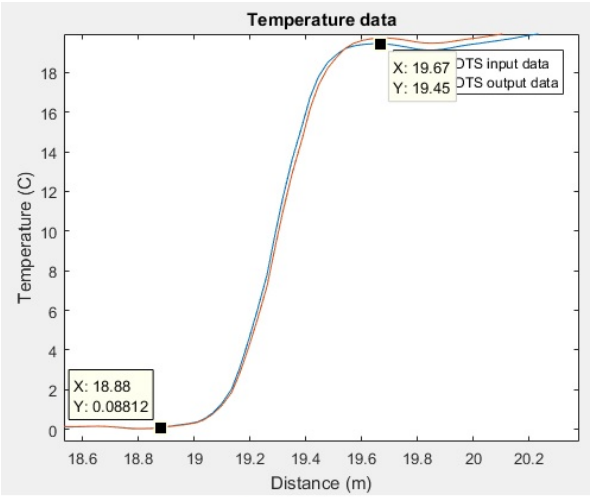

Figure 3-32: Machine resolution for Gaussian impulse response and spatial resolution of 3.15cm

The spatial resolution is finally increased by a factor of eight and the resulting machine resolution is shown in Figure 3-33. In this case the temperature estimate is for every 1.58cm The machine resolution is increased to 80cm. Compared to the machine resolution of 51cm this is a decrease of 31cm (58%).

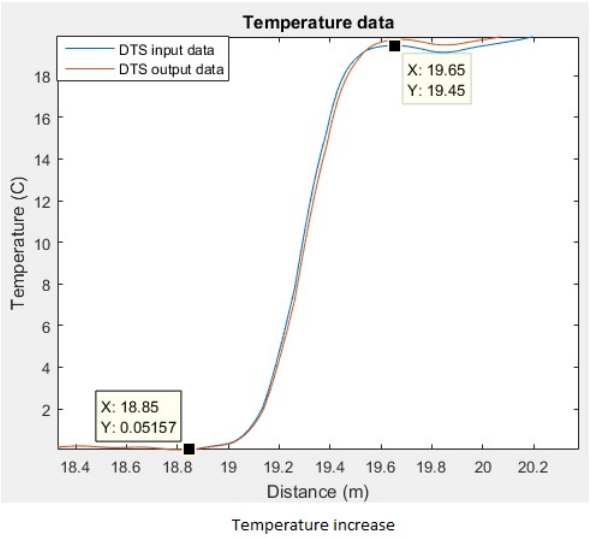

Figure 3-33: Machine resolution for Gaussian impulse response and spatial resolution of 1.58cm

Spatial-resolution (cm)	Machine-resolution (cm)	Machine-resolution decrease (cm)	Machine-resolution decrease
12.5	51	NA	NA
6.3	70	19	37%
3.15	78	27	53%
1.58	80	31	58%

Table 3-3: Summary resolution Gaussian impulse response

The spatial- and machine resolution results are summarized in Table 3-3. To validate the total variation deconvolution algorithm, the input temperature is estimated for another data set. This is shown in Figure 3-34.

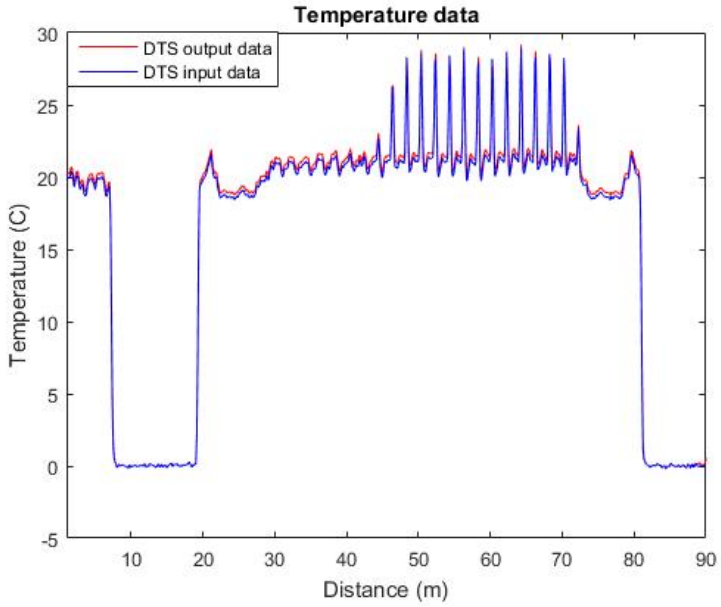

Figure 3-34: Input temperature with resolution 6.3cm and Gaussian impulse second measurement

From Figure 3-34 it is observed that the DTS input data is below the DTS output data. There is a difference of 0.27°C, which is the same as for the first data set. Moreover, the spikes between 50m and 80m are perfectly reconstructed. This means that the total variation deconvolution algorithm which is used to estimate the input temperature, is correct. In Figure 3-35 the machine resolution is shown. The machine resolution is 70cm, which is the same as for the first measurement when the spatial resolution is increased by a factor of two. When the spatial resolution is increased by a factor of four and a factor of eight, the machine resolution remains the same as for the first measurement, respectively 78cm and 80cm.

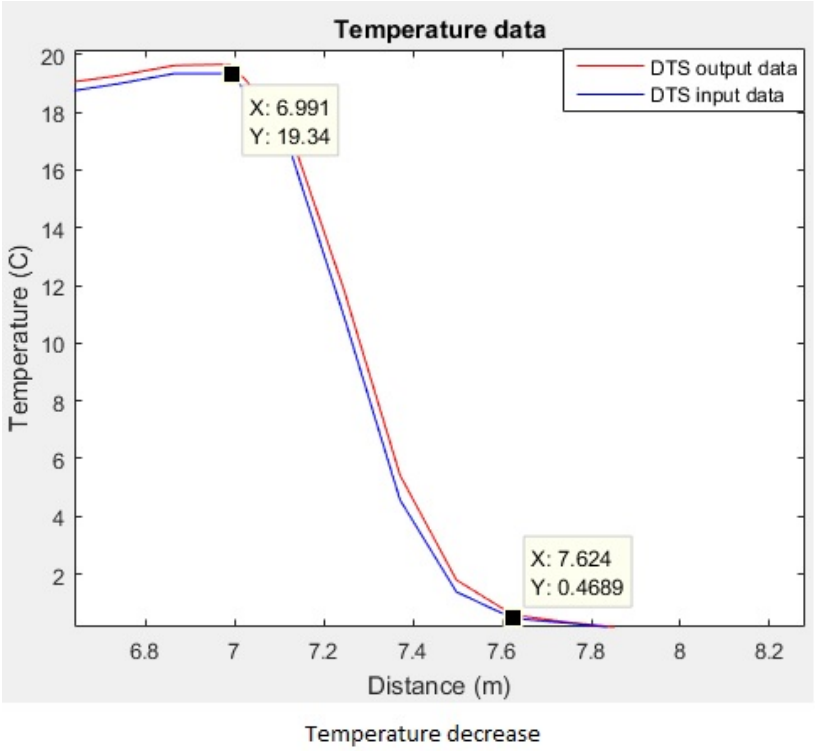

Figure 3-35: DTS machine resolution for Gaussian impulse response second measurement

Chapter 4

Conclusions and discussions

It is of utmost importance to monitor the temperature of patients inside a 7T MRI scanner because of the increased SAR level. The monitoring of the temperature should be realized with a spatial resolution as small as possible. In this thesis we have evaluated different methods for increasing the spatial resolution of an existing temperature sensing system. To this end we have evaluated the ideal input method, the blind deconvolution method and the Gaussian impulse response method. Also we have developed algorithms to estimate the real input temperature. These algorithms are the total variation deconvolution algorithm and the blind deconvolution algorithm. Finally, we conclude the following

1. **In order to estimate the impulse response it is not correct to assume ideal input temperature over the full cable length of 90m.**

   The input temperature is only known when the fiber optic cable is in the ice bath of approximately 0°C and therefore it cannot be assumed that the input temperature is ideal over the full cable length. It is only safe to assume known input temperature between 10-20m because at this distance the fiber optic cable is in an ice bath. Keeping in mind this assumption the impulse response can be estimated with the MLE method.

2. **Blind deconvolution algorithm can be used to obtain both the impulse response and input temperature as only the output temperature is known.**

   The blind deconvolution algorithm strongly depends on the initial guess of the impulse response. If the initial guess is not good the estimated impulse response will be bad. Because it is difficult to find a good initial guess of the impulse response, the blind deconvolution algorithm should be avoided in this case to estimate the impulse response.

3. **The ideal input method gives an accurate estimate of the input temperature by using the total variation deconvolution algorithm.**

   By assuming ideal input temperature between 10-20m, the total variation deconvolution algorithm filters out the measurement error in the output and also the machine resolution is increased with 19%.

Moreover, the input temperature is correctly estimated when the total variation deconvolution algorithm is used for different data sets. Hence, the total variation deconvolution algorithm is correct.

4. **The blind deconvolution algorithm does not give an accurate estimate of the input temperature but it does improve the machine resolution with 19%.**

   First of all, the blind deconvolution algorithm strongly depends on the initial guess of the impulse response. With this method it is very difficult to estimate the input temperature because it is difficult to find a good initial guess of the impulse response. Second, the blind deconvolution algorithm works in the Fourier domain and as a consequence of this, ringing effects are introduced. Due to ringing effects there is an overshoot of the temperature at the edges, which is not correct.

5. **The assumption that the DTS has a Gaussian impulse response gives an input temperature, by using the total variation deconvolution algorithm, which is similar to the input temperature obtained from the ideal input method. The machine resolution is also improved.**

   The ideal input method gives an exponential impulse response and therefore the Gaussian impulse response does not give the same input temperature as obtained with the ideal input method.

6. **The increase of the spatial resolution of the input temperature decreases the machine resolution for the ideal input method, blind deconvolution method and Gaussian impulse response.**

   The machine resolution decrease is the same for both the ideal input method and Gaussian impulse response. The blind deconvolution method deceases the machine resolution in the order of 400%.

Chapter 5

Future research

At the faculty of Civil Engineering of the Delft University of Technology it has been shown that the spatial resolution of the DTS measurement can be improved by using a dense array of fiber optic cables [12]. In [12] it is proposed to use a coil array to measure the temperature with a spatial resolution that depends on the machine resolution of the DTS and the diameter of the coil. In this thesis it has been shown that the machine resolution of the DTS can be improved to 51cm. From Eq. (3-1), it is derived that the coil diameter should be 10cm if we want to measure the temperature with a coil resolution of at least 5cm, as the machine resolution is 51cm. The coil diameter can be spread out over 5cm, in smaller coils of 2cm (5coils of 2cm) so that there is a temperature measurement for every 5cm. This is a spatial resolution increase of at least 7.6cm.

It should be further investigated if the proposed method indeed increases the spatial resolution of the temperature measurement. For this research a 3D coil geometry is proposed with a diameter of 2cm if the temperature measurement should have a spatial resolution requirement of, for example 5cm.

Recommendation

In this study it has been shown that the machine resolution became worse after increasing the spatial resolution by interpolation in the Fourier domain. Therefore, it is not recommended to perform interpolation but to use a more dense array of fiber optic cables (geometry as proposed here) in order to increase the spatial resolution.

Glossary

AWGN	Additive White Gaussian Noise
cm	Centimeter
DFB LD	Distributed Feedback Laser Diode
DTS	Distributed Temperature Sensing
FBG	Fiber Bragg Grating
FFT	Fast Fourier Transformation
FOS	Fiber Optic Sensor
IFFT	Inverse Fast Fourier Transformation
IRLS	Iterative Regularization Least Squares
LCFBG	Linearly Chirped Fiber Bragg Grating
LD	Laser Diode
LFMOW	Linearly Frequency Modulated Optical Waveform
LTI	Linear Time Invariant
m	Meter
MLE	Maximum Likelihood Estimation
MR	Magnetic Resonance
MRI	Magnetic Resonance Imaging
PD	Photo Diode
PRF	Pulse Repetition Frequency
SAR	Specific Absorption Rate
SNR	Signal to Noise Ratio
T	Tesla

Bibliography

[1] F. Taffoni, D. Formica, P. Saccomandi, G. Di Pino and E. Schena, "Optical Fiber Based MR-Compatible Sensors for Medical Applications: An Overview," *Sensors*, vol. 13, no. 10, pp. 14105-14120, Oct. 2013.

[2] R. R. Edelman and S. Warach, "Magnetic resonance imaging," *New England Journal of Medicine*, vol. 328, no. 10, pp. 708716, Mar. 1993.

[3] E. M. Merkle and B. M. Dale, "Abdominal MRI at 3.0 T: The basics revisited," *American Journal of Roentgenology*, vol. 186, no. 6, pp. 15241532, Jun. 2006.

[4] F. Thiel et al., "Implementation of ultra-wideband sensors for biomedical applications: Frequenz,*Frequenz*, vol. 63, no. 9-10, pp. 221224, Apr. 2013.

[5] M. F. Fahmy, G. M. A. Raheem, U. S. Mohamed, and O. F. Fahmy, "A new fast Iterative blind Deconvolution algorithm," *Journal of Signal and Information Processing*, vol. 03, no. 01, pp. 98-108, Jan. 2012.

[6] D. A. Krohn, T. MacDougall, A. Mendez, and Society of Photo-optical Instrumentation Engineers, *Fiber Optic Sensors Fundamentals and Applications*, 4th ed. 2014.

[7] W. W. Morey, G. Meltz and W. H. Glenn, "Fiber optic Bragg grating sensors," *Society of Photo-optical Instrumentation Engineers* Vol. 1169 Fiber Optic and Laser Sensors VII (1989) / 107.

[8] Y. Wang, J. Zhang, O. Coutinho and J. Yao, "Interrogation of a linearly chirped fiber Bragg grating sensor with high resolution using a linearly chirped optical waveform," *Optics Letters*, vol. 40, no. 21, p. 4923, Oct. 2015.

[9] S. D. Dyer, M. G. Tanner, B. Baek, R. H. Hadfield, and S. W. Nam, "Analysis of a distributed fiber-optic temperature sensor using single-photon detectors," *Optics Express*, vol. 20, no. 4, p. 3456, Jan. 2012.

[10] J. P. Bazzo, D. R. Pipa, C. Martelli, E. Vagner da Silva, and J. C. Cardozo da Silva, "Improving spatial resolution of Raman DTS using total variation Deconvolution," *IEEE Sensors Journal*, vol. 16, no. 11, pp. 44254430, Jun. 2016.

[11] K. Raeen, "A Study of The Gibbs Phenomenon in Fourier Series and Wavelets," 2008.

[12] K. Hilgersom, T. van Emmerik, A. Solcerova, W. Berghuijs, J. Selker, and N. van de Giesen: Practical considerations for enhanced-resolution coil-wrapped distributed temperature sensing, *Geosci. Instrum. Method. Data Syst.*, 5, 151-162, doi:10.5194/gi-5-151-2016, 2016.